mutation spectrum narrowed to T315I and E344V by direct sequencing, whereas, at intermediate concentration of AUY922, the resistant clone was recovered by wild-type (WT) BCR–ABL only. The observed data from the isobologram indicated the synergistic effect of simultaneous exposure to AUY922 and nilotinib even in BaF3 cells expressing BCR–ABL mutants including T315I. *In vivo* studies also demonstrated that the combination of AUY922 and nilotinib prolonged the survival of mice transplanted with mixture of BaF3 cells expressing WT BCR–ABL and mutant forms. Taken together, this study shows that the combination of AUY922 and nilotinib exhibits a desirable therapeutic index that can reduce the *in vivo* growth of mutant forms of BCR–ABL-expressing cells.

Results

AUY922 in combination with nilotinib or imatinib completely suppresses outgrowth of resistant clones by random mutagenesis screen

To assess whether combinations of ABL kinase inhibitors offer an advantage over AUY922 alone, we carried out a random mutagenesis screens with combinations of AUY922 and imatinib or nilotinib (Ray *et al.*, 2007). This approach uses a DNA repair-deficient *Escherichia coli* strain to produce random mutagenesis of a BCR–ABL retroviral plasmid, infection of BaF3 cells and selection for BaF3 clones conferring varying degree of drug resistance (Ray *et al.*, 2007). Profiling of AUY922 as a single agent revealed a concentration-dependent reduction of colonies (Figure 1). Sequencing revealed only WT BCR–ABL in AUY922-resistant clones, with the lowest concentration of AUY922 and 500 nM of imatinib (Figure 1). Sequencing of nilotinib-resistant clones with the highest concentration (2 μM) revealed T315I and E344V (Figure 1). We then performed a comprehensive drug combination using a broader range of concentrations of AUY922 and nilotinib or imatinib. Compared with single agent, combinations with AUY922 and nilotinib or AUY922 and imatinib were more effective at reducing the outgrowth of resistant clones. No outgrowth was observed in the presence of 2 μM of nilotinib and 20 nM of AUY922 (Figure 1).

Combined effects of AUY922 and nilotinib in mutant forms of BCR–ABL-expressing cells

We used the isobologram method to determine whether the combined effects of AUY922 and nilotinib are additive or synergistic in mutant forms of BCR–ABL-expressing BaF3 cells. Figure 2a showed the dose-response curve for AUY922 and nilotinib in WT-p210 BCR–ABL-expressing BaF3 cells. The isobologram was generated on the dose-response curve. The observed data from the isobologram indicated the synergistic effect on simultaneous exposure to AUY922 and nilotinib in WT BCR–ABL-expressing BaF3 cells (Figure 2a). M351T is a sensitive mutation to nilotinib, on the other hand, E255K is an insensitive mutation to

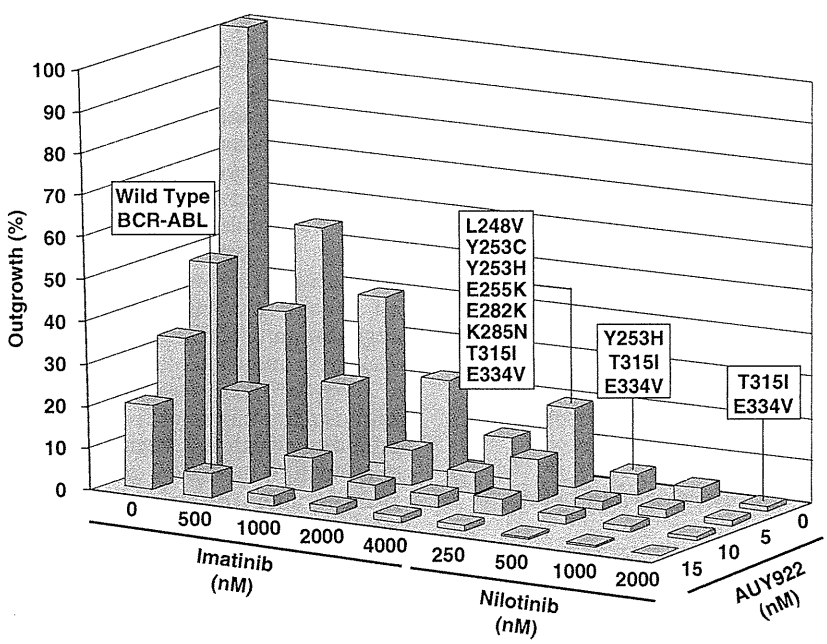

Figure 1 AUY922 in combination with nilotinib or imatinib completely suppresses outgrowth of resistant clones. The approach uses a DNA repair-deficient *Escherichia coli* strain to produce random mutagenesis of a BCR–ABL retroviral plasmid, infection of BaF3 cells, and selection for BaF3 clones conferring varying degree of drug resistance using methods previously described (Azam *et al.*, 2003). BaF3 cells expressing the random mutagenesis of BCR–ABL were kindly provided by Dr James D Griffin (Dana-Farber Cancer Institute) (Ray *et al.*, 2007). BaF3 cells expressing the random mutagenesis of a BCR–ABL were cultured with graded concentrations of AUY922 alone and in combination with imatinib or nilotinib. Bars represent the percentage of wells from which drug-resistant clones were recovered. Similar results were obtained in three independent experiments.

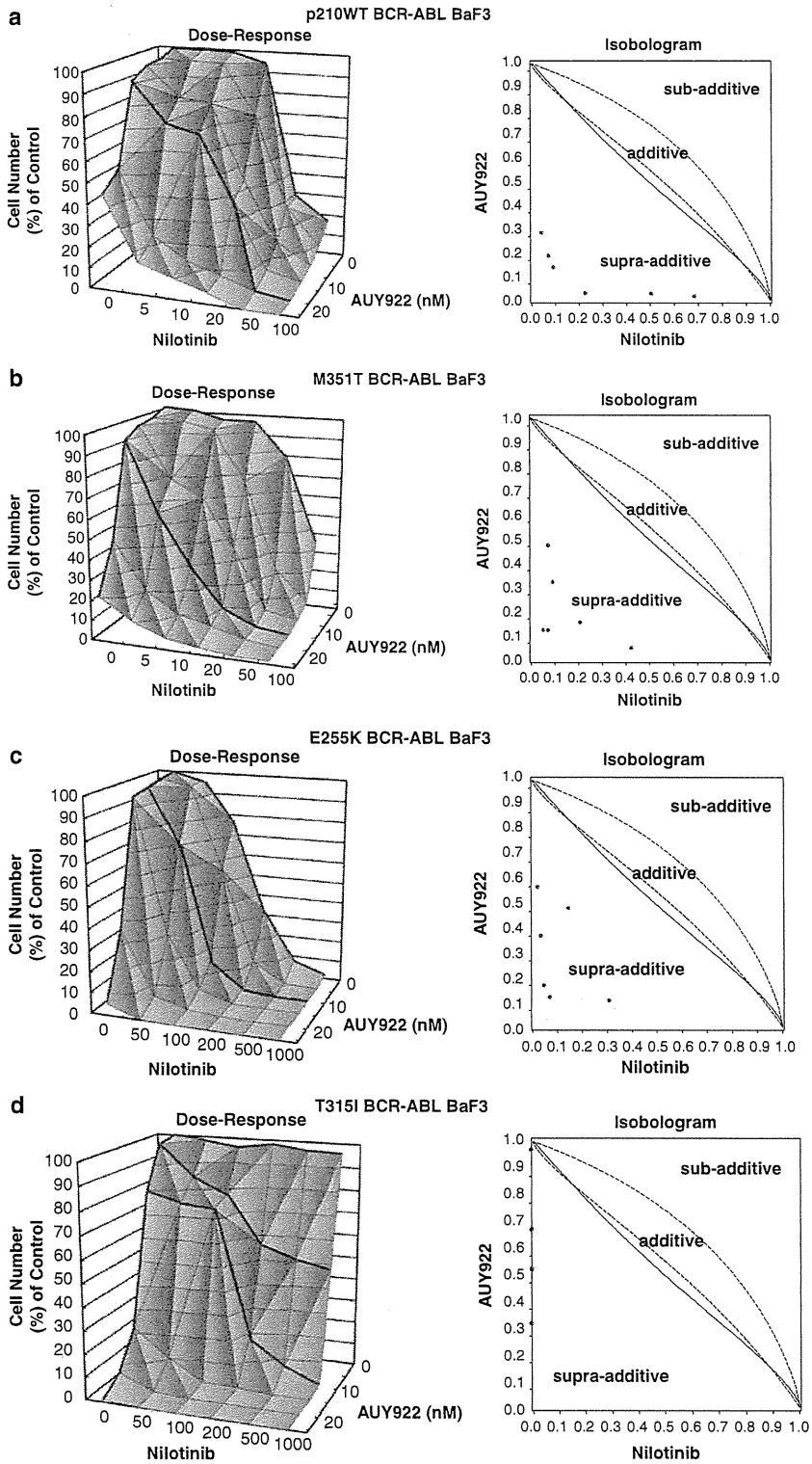

Figure 2 Combined effects of AUY922 and nilotinib in mutant forms of BCR–ABL-expressing cells. The theoretical basis of isobologram method and the procedure for making isobolograms have previously been described in detail (Kano *et al.*, 2001). The dose-response curves and generated isobologram for AUY922 and nilotinib were shown in Figure **a** (WT p210 BCR–ABL), **b** (M351T BCR–ABL), **c** (E255K BCR–ABL) and **d** (T315I BCR–ABL). The observed data from the isobologram indicated the synergistic effect of simultaneous exposure to AUY922 and nilotinib even in BaF3 cells expressing BCR–ABL mutants including T315I. Similar results were obtained in three independent experiments.

nilotinib. The isobolograms show the combination with AUY922 and nilotinib has the synergistic effect on both mutation (Figures 2b and c). In constant, T315I BaF3 cells were resistant to nilotinib up to levels as high as 2 μM, however, the treatment with AUY922 and nilotinib showed the synergistic effect in T315I BCR–ABL BaF3 cells (Figure 2d). Next, we determined the colony growth of WT BCR–ABL BaF3 cells and WT BCR–ABL-expressing primary chronic myeloid leukemia (CML) mononuclear cells (Figure 3a). Co-treatment with AUY922 and nilotinib caused significantly more inhibition of colony growth than treatment of either agent alone in WT BCR–ABL BaF3 cells and primary CML cells (Figure 3a). Further, we examined the colony growth of T315I BaF3 cells and T315I-expressing primary cells (Figure 3b). Co-treatment with AUY922 and nilotinib caused significantly more inhibition of colony growth than treatment of either agent alone in T315I BaF3 cells and T315I-expressing primary leukemia cells (Figure 3b). WT BCR–ABL BaF3 cells and

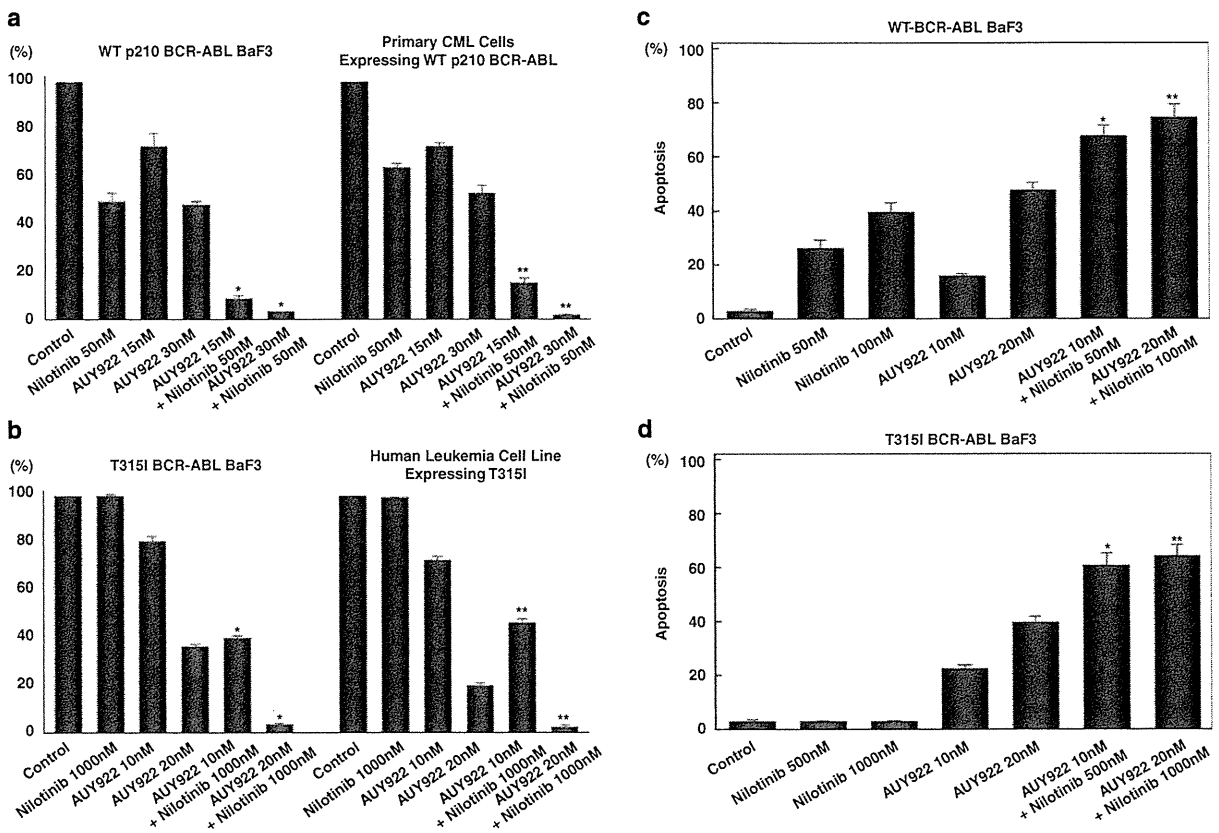

Figure 3 Co-treatment of AUY922 and nilotinib suppresses colony formation of in WT BCR–ABL and T315I BCR–ABL-expressing cells, and enhances the induction of apoptosis. (**a**) WT BCR–ABL BaF3 cells and WT BCR–ABL-expressing primary CML mononuclear cells were grown in methylcellulose containing the indicated concentrations of AUY922 and nilotinib. Colony counts were assessed on each individual sample at least twice, and results are presented as average ± s.d. for colonies counted from triplicate plates under each condition. WT BCR–ABL BaF3 cells; nilotinib 50 nM: 49.1 ± 3.5%, AUY922 15 nM: 73.5 ± 5.5%, AUY922 30 nM: 48.4 ± 1.4%, AUY922 15 nM + nilotinib 50 nM: 9.4 ± 0.3%, AUY922 30 nM + nilotinib 50 nM: 3.5 ± 0.1%, respectively. $*P<0.01$ compared with nilotinib 50 nM-treatment. WT BCR–ABL-expressing primary CML mononuclear cells; nilotinib 50 nM: 64.3 ± 1.9%, AUY922 15 nM: 73.3 ± 1.3%, AUY922 30 nM: 53.2 ± 3.1%, AUY922 15 nM + nilotinib 50 nM: 16.1 ± 1.8%, AUY922 30 nM + nilotinib 50 nM: 1.8 ± 0.1%, respectively. $**P<0.01$ compared with nilotinib 50 nM-treatment. (**b**) T315I BaF3 cells and T315I-expressing primary cells were grown in methylcellulose containing the indicated concentrations of AUY922 and nilotinib. Colony counts were assessed on each individual sample at least twice, and results are presented as average ± s.d. for colonies counted from triplicate plates under each condition. T315I BaF3 cells; nilotinib 1000 nM: 99.1 ± 0.8%, AUY922 10 nM: 81.5 ± 1.9%, AUY922 20 nM: 37.2 ± 0.8%, AUY922 10 nM + nilotinib 1000 nM: 40.2 ± 0.9%, AUY922 20 nM + nilotinib 1000 nM: 3.8 ± 0.2%, respectively. $*P<0.01$ compared with nilotinib 1000 nM-treatment. T315I-expressing primary cells; nilotinib 1000 nM: 99.2 ± 0.1%, AUY922 10 nM: 73.5 ± 1.3%, AUY922 20 nM: 20.1 ± 0.9%, AUY922 10 nM + nilotinib 1000 nM: 46.9 ± 1.4%, AUY922 20 nM + nilotinib 1000 nM: 2.1 ± 0.4%, respectively. $**P<0.01$ compared with nilotinib 1000 nM-treatment. WT BCR–ABL BaF3 cells (**c**) and T315I BaF3 cells (**d**) were cultured with the indicated concentrations of AUY922 and nilotinib for 72 h, after which the percentage of apoptotic cells was determined by annexin-V. (**c**) WT BCR–ABL BaF3 cells; control: 3.3 ± 0.8%, nilotinib 50 nM: 25.8 ± 2.2%, nilotinib 100 nM: 39.6 ± 2.7%: AUY922 10 nM: 14.3 ± 0.9%, AUY922 20 nM: 43.2 ± 3.2%, AUY922 10 nM + nilotinib 50 nM: 67.8 ± 3.2%, AUY922 20 nM + nilotinib 100 nM: 74.5 ± 4.4%, respectively. $*P<0.01$ compared with nilotinib 50 nM-treatment. $**P<0.01$ compared with nilotinib 100 nM-treatment. (**d**) T315I BaF3 cells; control: 2.1 ± 0.5%, nilotinib 500 nM: 2.0 ± 0.1%, nilotinib 1000 nM: 2.1 ± 0.1%, AUY922 10 nM: 22.9 ± 0.8%, AUY922 20 nM: 39.6 ± 1.9%, AUY922 10 nM + nilotinib 500 nM: 60.2 ± 3.9%, AUY922 20 nM + nilotinib 1000 nM: 62.4 ± 3.8%, respectively. $*P<0.01$ compared with nilotinib 500 nM-treatment. $**P<0.01$ compared with nilotinib 1000 nM-treatment.

T315I BaF3 cells were cultured with the indicated concentrations of AUY922 and nilotinib for 72 h, after which the percentage of apoptotic cells was determined by annexin-V (Figures 3c and d). When 10 nM of AUY922 was combined with nilotinib in WT BCR–ABL BaF3 cells, the increase in apoptotic cells was virtually complete for nilotinib concentrations higher than 1 μM (Figure 3c). Treatment with 1 μM of nilotinib had no effect on T315I BaF3 cells, however, co-treatment of AUY922 and nilotinib also enhanced the induction of apoptosis in T315I BaF3 cells (Figure 3d). Together, these findings indicate that combination of minimally toxic concentrations of AUY922 and nilotinib is effective in inducing apoptosis in both WT BCR–ABL-expressing cells and T315I BCR–ABL-expressing cells.

AUY922 induces degradation of WT and mutant forms of BCR–ABL proteins

Previous studies have shown that the HSP90 inhibitors geldanamycine and 17-AAG disrupt HSP90 function and induce BCR–ABL degradation (Gorre *et al*., 2002). To determine whether AUY922 can similarly cause the degradation of BCR–ABL proteins, WT, T315I, E255K or M351T BCR–ABL-expressing BaF3 cells were exposed to varying concentrations of AUY922 for 24 h (Figures 4a and b). Immunoblot analysis revealed that AUY922 caused BCR–ABL protein levels to decrease significantly in WT BCR–ABL-expressing BaF3 cells at a dose of 50 nM, as expected (Figure 4a). Mutant forms of BCR–ABL proteins were also degraded at a lower concentration of AUY922 (Figures 4a and b). These results suggest that AUY922 may have greater potency against mutant forms of BCR–ABL proteins compared with WT.

The mechanism of the synergism between AUY922 and nilotinib in T315I BCR–ABL BaF3 cells

We next conducted the experiments to further evaluate the mechanism of the synergism between AUY922 and nilotinib in T315I BCR–ABL BaF3 cells. Besides the ABL kinases, the receptor tyrosine kinase DDR1 and the oxidoreductase NQO2 are target molecules for nilotinib (Bantscheff *et al*., 2007; Rix *et al*., 2007). T315I BaF3 cells were cultured with the indicated concentrations of nilotinib for 24 h, the cell lysates were

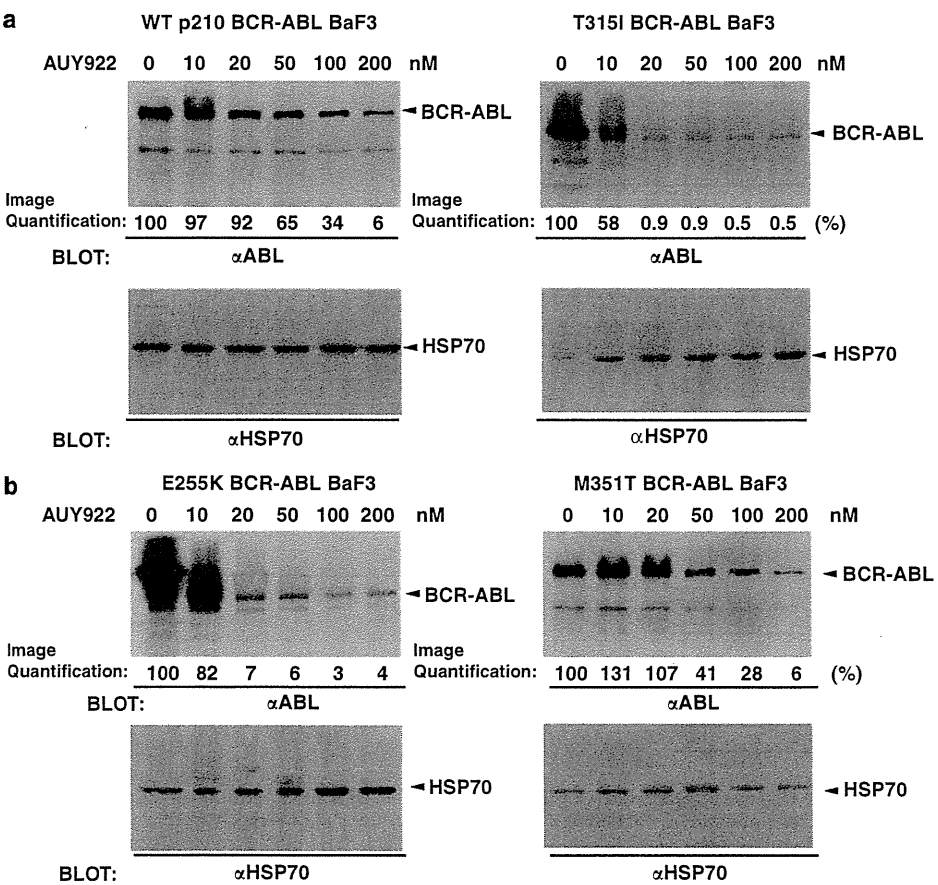

Figure 4 AUY922 induces degradation of WT and mutant forms of BCR–ABL proteins. (**a**) WT or T315I BCR–ABL-expressing BaF3 cells were exposed to varying concentrations of AUY922 for 24 h. The cell lysates were immunobloted with anti-ABL Ab or anti-HSP70 Ab. (**b**) E255K, or M351T BCR–ABL-expressing BaF3 cells were exposed to varying concentrations of AUY922 for 24 h. The cell lysates were immunobloted with anti-ABL Ab or anti-HSP70 Ab.

immunoprecipitated with anti-DDR1 antibody (Ab) and then immunoblotted with anti-phosphotyrosine mAb (PY20) or anti-DDR1 Ab (Figure 5a). Higher concentrations of nilotinib abolished DDR1 autophosphorylation (Figure 5a). To assess the functional importance of DDR1 and NQO2, we used RNA interference to determine whether reduction in DDR1 and NQO2 affect the proliferation of T315I BaF3 cells after the treatment of AUY922. T315I BaF3 cells were transfected with control small interfering RNA (siRNA) or *DDR1* siRNA or *NQO2* siRNA; then the DDR1 and NQO2 expression was analyzed by immunoblotting after 48 h (Figure 5b). At 48 h after transfection, T315I BCR–ABL BaF3 cells were treated with indicated concentration of AUY922 for 48 h, and viable cells were counted (Figure 5c). In the presence of *DDR1* siRNA, T315I BCR–ABL BaF3 cells increased antiproliferative activity with AUY922 (at 5 or 10 nM) (Figure 5c). When AUY922 was treated in the presence of *NQO2* siRNA, antiproliferative activity of T315I BCR–ABL was not observed (Figure 5c). These results showed that inhibition of DDR1 can have an important role in the synergism between AUY922 and nilotinib.

Further, we examined the phosphorylation of T315I BCR–ABL after treatment of AUY922 and nilotinib. T315I BCR–ABL BaF3 cells were cultured with indicated concentrations of AUY922 and nilotinib for 24 h. The cell lysates were immunoblotted with anti-phosho-ABL Ab or anti-ABL Ab (Figure 5d). Co-treatment with AUY922 and nilotinib partially decreased auto-phosphorylation of T315I BCR–ABL (Figure 5d).

Co-treatment of AUY922 and nilotinib prolong the survival in mice model of BCR–ABL mutant-induced leukemia

We investigate the *in vivo* efficacy of AUY922 and nilotinib (Figure 6). Twelve-week-old nude mice were injected with 5×10^5 cells of mixture of BaF3 cells expressing WT BCR–ABL and mutant forms of BCR–ABL (M244V, G250E, Q252H, Y253F, T315A, T315I, F317L, F317V, M351T and H396P). At 24-h injection of the leukemia cells, these mice were treated with either vehicle or AUY922 (50 mg/kg intraperitoneal (i.p.); two times per week) or nilotinib (30 mg/kg; q.d.) or AUY922 (50 mg/kg i.p.; two times per week) + nilotinib

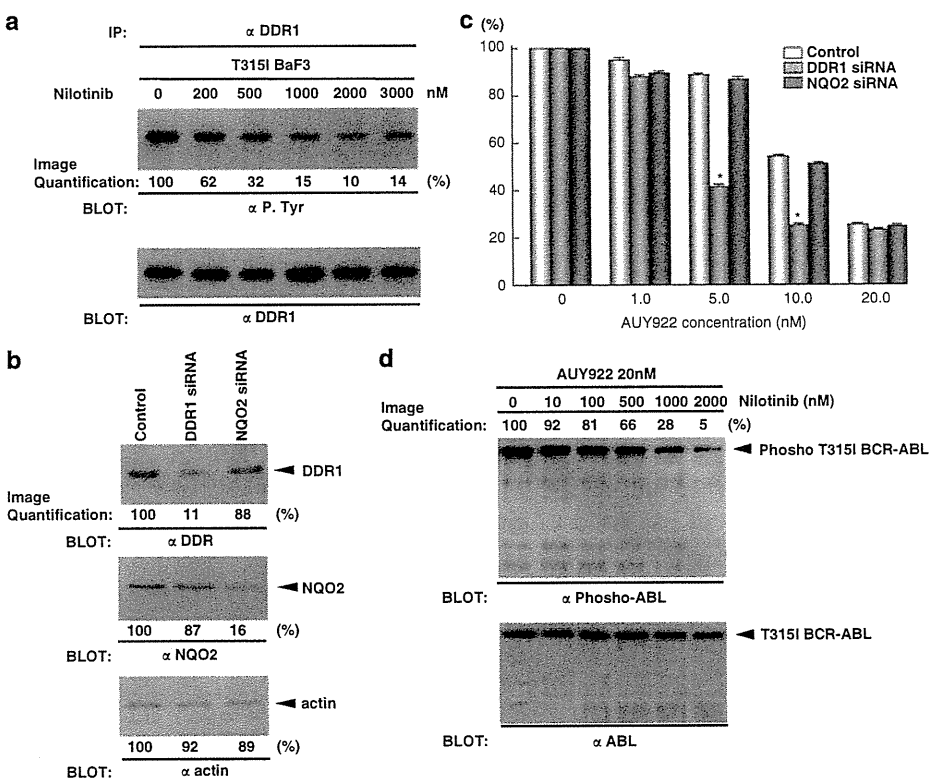

Figure 5 The mechanism of the synergism between AUY922 and nilotinib in T315I BCR–ABL BaF3 cells. (**a**) T315I BaF3 cells were cultured with the indicated concentrations of nilotinib for 24 h, the cell lysates were immunoprecipitated with anti-DDR1 Ab and then immunoblotted with anti-phosphotyrosine mAb or anti-DDR1 Ab. (**b**) T315I BaF3 cells were transfected with control siRNA or *DDR1* siRNA or *NQO2* siRNA; then the DDR1 and NQO2 expression was analyzed by immunoblotting after 48 h. (**c**) At 48 h after transfection, T315I BCR–ABL BaF3 cells were treated with indicated concentration of AUY922 for 48 h, and viable cells were counted by using Vi-cell XR automated cell viability analyzer (Beckman Coulter). The mean number of viable cells at different concentration of drug was normalized to the mean number of viable cells in the no-drug samples. $^*P<0.01$ compared with contro siRNA-treatment. Similar results were obtained in each of three independent experiments. (**d**) T315I BCR–ABL BaF3 cells were cultured with indicated concentrations of AUY922 and nilotinib for 24 h. The cell lysates were immunoblotted with anti-phosho-ABL Ab or anti-ABL Ab.

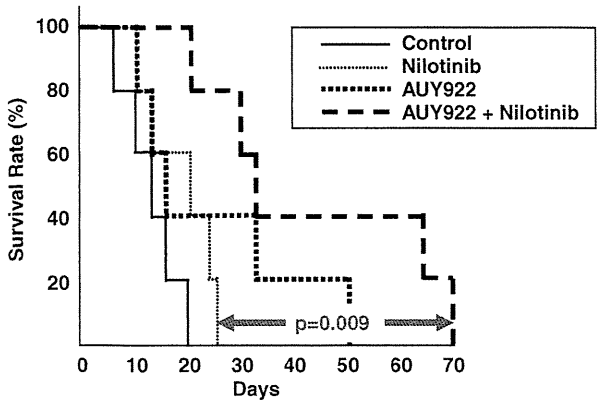

Figure 6 Co-treatment of AUY922 and nilotinib prolong the survival in mice model of BCR–ABL mutant-induced leukemia. Nude mice were injected with 5×10^5 cells of mixture of BaF3 cells expressing WT BCR–ABL and mutant forms of BCR–ABL (M244V, G250E, Q252H, Y253F, T315A, T315I, F317L, F317V, M351T and H396P). At 24-h injection of the leukemia cells, these mice were treated with either vehicle or AUY922 (50 mg/kg i.p.; two times per week) or nilotinib (30 mg/kg; q.d.) or AUY922 (50 mg/kg i.p.; two times per week) + nilotinib (30 mg/kg; q.d.).

(30 mg/kg; q.d.). The vehicle or nilotinib-treated mice died of a condition resembling acute leukemia by 28 days; the combination of AUY922 + nilotinib-treated mice survived more than 60 days, significantly improved the survival ($P = 0.009$) compared with nilotinib-treated mice (Figure 6).

Discussion

Second-generation TKIs have demonstrated increased inhibitory potency against BCR–ABL tyrosine kinase and have shown efficacy in treating patients with number of the BCR–ABL kinase domain mutations that develop on imatinib (Kantarjian *et al.*, 2006, 2007, 2009; Ottmann *et al.*, 2007). Despite the significant clinical activity demonstrated in clinical trials, a number of patients do not show durable response (Garg *et al.*, 2009). One reason for the lack of durable response could be explained by the emergence of new kinase domain mutations as patients are exposed to sequential TKIs (Branford *et al.*, 2009; Garg *et al.*, 2009). The challenge for development of an effective Ph-positive leukemia therapy is therefore to develop an alternative treatment strategy that does not rely solely on kinase domain inhibition but rather results in degradation of the offending BCR–ABL protein regardless of its mutation status.

AUY922 is a most potent resorcinylic isoxazole amide HSP90 inhibitor, which binds to the adenosine triphosphate-binding pocket of HSP90 (Brough *et al.*, 2008). AUY922 has excellent cellular potency against a panel of tumor cell lines (Brough *et al.*, 2008; Eccles *et al.*, 2008; Stuhmer *et al.*, 2008). In addition, optimization of pharmacokinetic properties led to robust therapeutic responses in a wide variety of human tumor xenografts tightly linked to high intratumor concentrations of compound and phamacodynamic response (Eccles *et al.*, 2008). The promising preclinical data obtained with AUY922 supported the initiation of clinical phase I trials in patients with solid tumors.

In this study, we investigated a comprehensive drug combination experiment using a broader range of concentrations for AUY922 and nilotinib or imatinib by saturation mutagenesis screen (Figure 1). AUY922 controlled the outgrowth of WT BCR–ABL, and mutated forms of BCR–ABL associated with imatinib or nilotinib resistance (Figure 1). When AUY922 was included with imatinib or nilotinib, outgrowth of resistant subclones were significantly reduced (Figure 1). Although further pharmacokinetic analysis of AUY922 will be necessary, it is remarkable that even the lowest dose of AUY922 tested in combination with clinically relevant concentrations of nilotinib completely suppressed the emergence of resistant clone.

The T315I BCR–ABL mutation is emerging as a common mechanism of failure to second line ABL TKIs. Thus, even in advanced phase of CML, BCR–ABL remains the critical therapeutic target. So far, reports of successful salvage therapy for CML patients who acquire the T315I BCR–ABL mutation are limited to small clinical trials. The isobologram analysis indicated the synergistic effect of simultaneous exposure to AUY922 and nilotinib even in BaF3 cells expressing BCR–ABL mutants including T315I (Figure 2). Further, combination of AUY922 and nilotinib is also effective in inducing apoptosis in both WT BCR–ABL-expressing cells and T315I BCR–ABL-expressing cells (Figures 3c and d). These results indicate that co-treatment with AUY922 sensitizes T315I BCR–ABL-expressing cells to clinically achievable trough levels of nilotinib. However, the structural basis for how co-treatment with AUY922 leads to enhanced activity of nilotinib against the gatekeeper T315I BCR–ABL mutant is entirely unclear. It is possible that nilotinib may collaborate with AUY922 in significantly inhibiting the off-target tyrosine kinase besides BCR–ABL. DDR1 is thought to transducer signals to NFκB pathway (Matsuyama *et al.*, 2004). Higher concentrations of nilotinib abolished DDR1 phosphorylation (Figure 5a). Further, down regulation of *DDR1* by siRNA increased antiproliferative activity in AUY922-treated T3151 BCR–ABL BaF3 cells (Figure 5c). Our results clearly show that DDR1 may contribute at least in part to the synergism between AUY922 and nilotinib. Alternative possibility is that AUY922-mediated inhibition of HSP90 chaperon function for BCR–ABL affects the conformational change of BCR–ABL that allows higher concentrations of nilotinib to interact with T315I BCR–ABL. Co-treatment with AUY922 and nilotinib partially decreased autophosphorylation of T315I BCR–ABL (Figure 5d). In this regard, it is interesting to test whether AUY922 might influence the conformational dynamics of the adenosine triphosphate-binding site of

the 'gatekeeper' mutant, T315I BCR–ABL. Further studies are required to resolve these mechanisms.

The simultaneous use of AUY922 and nilotinib in chronic phase CML patients might prevent the development of nilotinib-resistant clones and inhibit growth of highly proliferative leukemia cells through inhibition of kinase activity, thereby providing a rationale for combination strategy. In a survival mouse model using BaF3 cells expressing WT BCR–ABL and mutant forms of BCR–ABL (M244V, G250E, Q252H, Y253F, T315A, T315I, F317L, F317V, M351T and H396P), co-treatments with AUY922 and nilotinib significantly improved the survival ($P = 0.009$) (Figure 6). The results from these studies suggest that combined use of AUY922 and nilotinib would be a viable strategy for preventing emergence of resistant clones in clinic.

In summary, our preclinical results indicate that AUY922 has potential as an important option for controlling resistance in CML. The combined results of cell-based and *in vivo* studies suggest that AUY922 exhibits sufficient activity against mutants form of BCR–ABL to warrant consideration for combined use with ABL TKIs. Although several HSP90 inhibitors have now entered clinical evaluation, it is expected that through new formulations of AUY922, orally administrable, it will be more favorably modulate the schedule for CML patients.

Materials and methods

Antibodies and reagents
Anti-ABL Ab (24-11), anti-HSP70 Ab, anti-DDR1 Ab and anti-NQO2 Ab were purchased from Santa Cruz Biotechnology, Inc. (Santa Cruz, CA, USA). Anti-phosphotyrosine mAb (PY20) was purchased from Becton Dickinson and Company (Franklin Lakes, NJ, USA). Anti-phospho-ABL Ab was obtained from Cell Signaling (Beverly, MA, USA). AUY922, nilotinib and imatinib were kindly provided by Novartis Pharma AG (Basel, Switzerland).

Cells and cell culture
The approach uses a DNA repair-deficient *E. coli* strain to produce random mutagenesis of a BCR–ABL retroviral plasmid, infection of BaF3 cells, and selection for BaF3 clones conferring varying degree of drug resistance. BaF3 cells expressing the random mutagenesis of BCR–ABL were kindly provided by Dr James D Griffin (Dana-Farber Cancer Institute, Boston, MA, USA) (Ray *et al.*, 2007). BaF3 cells expressing WT BCR–ABL and mutant forms of BCR–ABL (M244V, G250E, Q252H, Y253F, T315A, T315I, F317L, F317V, M351T and H396P) were described previously (Deguchi *et al.*, 2008). These cell lines were cultured in RPMI1640 (Life Technology, Inc., Carlsbad, CA, USA) supplemented with 10% fetal calf serum (Hyclone Laboratories, Logan, UT, USA).

The isobologram method
The theoretical basis of isobologram method and the procedure for making isobolograms have previously been described in detail (Kano *et al.*, 2001). Cells were suspended to a final concentration of 1×10^5 cells/ml in fresh medium, plated in 24-well dishes and incubated with AUY922 or imatinib or nilotinib or in combination at 37 °C for 72 h. The number of cells in each well was counted by flow cytometry, and the cell numbers were normalized by dividing the number of cells (Nunoda *et al.*, 2007).

Apoptosis assay
The cells were treated with the indicated concentration of AUY922 and/or nilotinib for 48 h. Annexin V/propidium iodide apoptosis assay was performed according to the manufacturer's protocol (Becton Dickinson and Company). The cells were gently mixed and immediately analyzed by flow cytometry.

Immunoblotting
Immunoblotting was performed as described previously (Tauchi *et al.*, 1994).

siRNA experiments
siRNA oligonucleotides for murine *DDR1* and *NQO2* were purchased from Santa Cruz Biotechnology, Inc., and resuspended in RNase-free H2O at 20 μM. siRNA (1.25 μM) was added to prechilled 0.4 cm-gap electroporation cuvetts (Bio-Rad, Hercules, CA, USA). T315I BaF3 cells (5×10^6) were washed twice in serum-free media and resuspended to 5×10^6 cells per 250 μl of cold, serum-free RPMI 1640. Cells were added to the cuvetts, mixed, and mixed on ice for 5 min. Cells were then pulsed once at 250 mV, 960 μF and 200 ohms by using a Bio-Rad electroporator. At 48 h after electroporation, protein knockdown was determined by immunoblotting, and cells were treated with the indicated concentration of dasatinib or imatinib for 48 h, viable cells were counted by using a Vi-cell XR automated cell viability analyzer (Beckman Coulter, Brea, CA, USA). The mean number of viable cells at varying concentrations of drug was normalized to the mean number of viable cells in the no-drug sample.

In vivo *experiments*
Twelve-week-old nude mice were injected with 5×10^5 cells of mixture of BaF3 cells expressing WT BCR–ABL and mutant forms of BCR–ABL (M244V, G250E, Q252H, Y253F, T315A, T315I, F317L, F317V, M351T and H396P). At 24-h injection of the leukemia cells, these mice were treated with either vehicle or AUY922 (50 mg/kg i.p.; two times per week) or nilotinib (30 mg/kg; q.d.) or AUY922 (50 mg/kg i.p.; two times per week) + nilotinib (30 mg/kg; q.d.). Mice were observed daily, and body weights as well as signs of stress (for example, lethargy, ruffled coat or ataxia) were used to detect possible toxicities.

Conflict of interest

TT receives research support from Novartis Pharma K.K.

Acknowledgements

This work was supported by a 'High-Tech Research Center' Project for private universities: matching fund subsidy from the MEXT (Ministry of Education, Culture, Sports, Science and Technology), and by the 'University-Industry Joint Research Project' for private universities: matching fund subsidy from the MEXT.

References

Azam M, Latek R, Daley GQ. (2003). Mechanisms of autoinhibition and STI-571/imatinib resistance revealed by mutagenesis of BCR-ABL. *Cell* **112**: 831–843.

Bantscheff M, Eberhard D, Abraham Y, Bastuck S, Boesche M, Hobson S *et al.* (2007). Quantitative chemical proteomics reveals mechanisms of action of clinical ABL kinase inhibitors. *Nat Biotech* **25**: 1035–1044.

Branford S, Melo JV, Hughes PT. (2009). Selecting optimal second-line tyrosine kinase inhibitor therapy for chronic myeloid leukemia patients after imatinib failure: does the BCR-ABL mutation status really matter? *Blood* **114**: 5426–5435.

Brough PA, Aherne W, Barril X, Borgogononi J, Boxall K, Cansfield JE *et al.* (2008). 4,5-Diarylisoxazole Hsp90 chaperone inhibitors: potential therapeutic agents for the treatment of cancer. *J Med Chem* **51**: 196–218.

Deguchi Y, Kimura S, Ashihara E, Niwa T, Hodohara K, Fujiyama Y *et al.* (2008). Comparison of imatinib, dasatinib, nilotinib and INNO-406 in imatinib-resistant cell lines. *Leuk Res* **32**: 980–983.

Eccles SA, Massey A, Raynaud FI, Sharp SY, Box G, Valenti M *et al.* (2008). NVP-AUY922: a novel heat shock protein 90 inhibitor active against xenograft tumor growth, angiogenesis, and metastasis. *Cancer Res* **68**: 2850–2860.

Garg RJ, Kantarjian H, O'Brien S, Quintas-Cardama A, Faderl S, Estrov Z *et al.* (2009). The use of nilotinib or dasatinib after failure to 2 prior tyrosine kinase inhibitors: long-term follow-up. *Blood* **114**: 4361–4368.

Gorre ME, Ellwood-Yen K, Chiosis G, Rosen N, Sawyers CL. (2002). BCR-ABL point mutants isolated from patients with imatinib mesylate-resistant chronic myeloid leukemia remain sensitive to inhibitors of the BCR-ABL chaperone heat shock protein 90. *Blood* **100**: 3041–3044.

Jabbour E, Kantarjian H, Jones D, Breeden M, Garcia-Manero G, O'Brien S *et al.* (2008). Characteristics and outcomes of patients with chronic myeloid leukemia and T315I mutation following failure of imatinib mesylate therapy. *Blood* **112**: 53–55.

Kano Y, Akutsu M, Tsunoda S, Mano H, Sato Y, Honma Y *et al.* (2001). In vitro cytotoxic effects of a tyrosine kinase inhibitor STI571 in combination with commonly used antileukemic agents. *Blood* **97**: 1999–2007.

Kantarjian H, Cortes J, Kim D-W, Dorlhiac-Llacer P, Pasquini R, DiPersio J *et al.* (2009). Phase 3 study of dasatinib 140 mg once daily versus 70 mg twice daily in patients with chronic myeloid leukemia in accelerated phase resistant or intolerant to imatinib: 15-month median follow-up. *Blood* **113**: 6322–6329.

Kantarjian H, Giles F, Wunderle L, Bhalla K, O'Brian S, Wassmann B *et al.* (2006). Nilotinib in imatinib-resistant CML and Philadelphia chromosome-positive ALL. *N Engl J Med* **354**: 2542–2551.

Kantarjian H, Pasquini R, Hamerschlak N, Rousselot P, Holowiecki P, Jootar S *et al.* (2007). Dasatinib or high-dose imatinib for chronic-phase chronic myeloid leukemia after failure of first-line imatinib: a randomized phase 2 trial. *Blood* **109**: 5143–5150.

Matsuyama W, Wang L, Farrar WL, Faure M, Yoshimura T. (2004). Activation of discoidin domain receptor 1 isoform b with collagen up-regulates chemokine production in human macrophages: role of p38 mitogen-activated protein kinase and NF-kappa B. *J Immunol* **172**: 2332–2340.

Nunoda K, Tauchi T, Takaku T, Okabe S, Akahane D, Sashida G *et al.* (2007). Identification and functional signature of genes regulated by structurally different ABL kinase inhibitors. *Oncogene* **26**: 4179–4188.

O'Hare T, Eide CA, Deininger MWN. (2007). Bcr-Abl kinase domain mutations, drug resistance, and the road to a cure for chronic myeloid leukemia. *Blood* **110**: 2242–2249.

Ottmann O, Dombret H, Martinelli G, Simonsson B, Guilhot F, Larson RA *et al.* (2007). Dasatinib induces rapid hematologic and cytogenetic responses in adult patients with Philadelphia chromosome positive acute lymphoblastic leukemia with resistance or intolerance to imatinib: interim results of a phase 2 study. *Blood* **110**: 2309–2315.

Ray A, Cowan-Jacob SW, Manley PW, Mestan J, Griffin JD. (2007). Identification of BCR-ABL point mutations conferring resistance to the Abl kinase inhibitor AMN107 (nilotinib) by a random mutagenesis study. *Blood* **109**: 5011–5015.

Rix U, Hantschel O, Dumberger G, Remsing Rix LL, Planyavsky M, Feenbach NV *et al.* (2007). Chemical proteomic profiles of the BCR-ABL inhibitors imatinib, nilotinib, and dasatinib reveal novel kinase and nonkinase targets. *Blood* **110**: 4055–4063.

Shah NP, Tran C, Lee FY, Chen P, Norris D, Saywers CL. (2004). Overriding imatinib resistance with a novel ABL kinase inhibitor. *Science* **305**: 399–401.

Stuhmer T, Zollinger A, Siegmund D, Chatterjee M, Grella E, Knop S *et al.* (2008). Signalling profile and antitumour activity of the novel Hsp90 inhibitor NVP-AUY922 in multiple myeloma. *Leukemia* **22**: 1604–1612.

Tauchi T, Boswell HS, Leibowitz D, Broxneyer HE. (1994). Coupling between p210bcr-abl and Shc and Grb2 adaptor proteins in hematopoietic cells permits growth factor receptor-independent link to ras activation pathway. *J Exp Med* **179**: 167–175.

Weisberg E, Manley PW, Breitenstein W, Bruggen J, Cowan-Jacob SW, Ray A *et al.* (2005). Characterization of AMN107, a selective inhibitor of native and mutant Bcr-Abl. *Cancer Cell* **7**: 129–141.

OPEN ACCESS Freely available online

PLoS one

15-Deoxy-$\Delta^{12,14}$ Prostaglandin J_2 Reduces the Formation of Atherosclerotic Lesions in Apolipoprotein E Knockout Mice

Takahiro Seno[1], Masahide Hamaguchi[2], Eishi Ashihara[3], Masataka Kohno[1], Hidetaka Ishino[1], Aihiro Yamamoto[1], Masatoshi Kadoya[1], Kaoru Nakamura[1], Ken Murakami[1], Satoaki Matoba[4], Taira Maekawa[5], Yutaka Kawahito[1]*

1 Department of Inflammation and Immunology, Graduate School of Medical Science, Kyoto Prefectural University of Medicine, Kyoto, Japan, **2** World Premier International Research Center, Immunology Frontier Research Center, Osaka University, Osaka, Japan, **3** Department of Molecular Cell Physiology, Graduate School of Medical Science, Kyoto Prefectural University of Medicine, Kyoto, Japan, **4** Department of Cardiovascular Medicine, Graduate School of Medical Science, Kyoto Prefectural University of Medicine, Kyoto, Japan, **5** Department of Transfusion Medicine and Cell Therapy, Kyoto University Hospital, Kyoto, Japan

Abstract

Aim: 15-Deoxy-$\Delta^{12,14}$ Prostaglandin J_2 (15d-PGJ_2) is a ligand of peroxisome proliferator-activated receptor γ (PPARγ) having diverse effects such as the differentiation of adipocytes and atherosclerotic lesion formation. 15d-PGJ_2 can also regulate the expression of inflammatory mediators on immune cells independent of PPARγ. We investigated the antiatherogenic effect of 15d-PGJ_2.

Methods: We fed apolipoprotein (apo) E-deficient female mice a Western-type diet from 8 to 16 wk of age and administered 1 mg/kg/day 15d-PGJ_2 intraperitoneally. We measured atherosclerotic lesions at the aortic root, and examined the expression of macrophage and inflammatory atherosclerotic molecules by immunohistochemical and real-time PCR in the lesion.

Results: Atherosclerotic lesion formation was reduced in apo E-null mice treated with 15d-PGJ_2, as compared to in the controls. Immunohistochemical and real-time PCR analyses showed that the expression of MCP-1, TNF-α, and MMP-9 in atherosclerotic lesions was significantly decreased in 15d-PGJ_2 treated mice. The 15d-PGJ_2 also reduced the expression of macrophages and RelA mRNA in atherosclerotic lesions.

Conclusion: This is the first report 15d-PGJ_2, a natural PPARγ agonist, can improve atherosclerotic lesions in vivo. 15d-PGJ_2 may be a beneficial therapeutic agent for atherosclerosis.

Citation: Seno T, Hamaguchi M, Ashihara E, Kohno M, Ishino H, et al. (2011) 15-Deoxy-$\Delta^{12,14}$ Prostaglandin J_2 Reduces the Formation of Atherosclerotic Lesions in Apolipoprotein E Knockout Mice. PLoS ONE 6(10): e25541. doi:10.1371/journal.pone.0025541

Editor: Massimo Federici, University of Tor Vergata, Italy

Received March 14, 2011; **Accepted** September 7, 2011; **Published** October 7, 2011

Funding: These authors have no support or funding to report.

Competing Interests: The authors have declared that no competing interests exist.

* E-mail: kawahity@koto.kpu-m.ac.jp

Introduction

Atherosclerosis is now recognized as a chronic inflammatory condition and remains the major cause of cardiovascular disease [1]. Over the past two decades, data have emerged showing that immune cells, especially macrophages, are involved in the formation of atherosclerotic plaques.

Peroxisome proliferator-activated receptor γ (PPARγ) is a member of the nuclear receptor superfamily, and is expressed in arterial wall cells, such as vascular smooth muscle cells, and macrophages [2]. Thiazolidinediones (TZDs), which are some of the most common PPARγ ligands, are insulin-sensitizing antidiabetic agents causing the improvement of hypertension and hypertriglyceridemia, both of which represent major risk factors for atherosclerosis. TZDs can improve atherosclerosis by decreasing these risk factors. A previous study indicated that troglitazone, a TZD, had pleiotropic anti-atherosclerotic effects on the expression of CD36 in atherosclerotic lesions and the serum level of HDL, but the details of the mechanisms were not clear [3]. Another function of TZDs comprises its anti-mitogenic effect on vascular smooth muscle cells [4]. TZDs also inhibit macrophage activation [5], monocyte migration [6], inflammatory cytokine secretion by monocytes [7–9], and the expression of cell adhesion molecules expressed by vascular endothelial cells [10,11]. Thus, a variety of anti-atherosclerotic effects of TZDs are associated with the regulation of inflammation caused by macrophages, but elucidation of the mechanisms in detail is required.

The J series of prostaglandins (PGs) have been demonstrated to regulate processes like inflammation and tumorgenesis [12]. 15-Deoxy-$\Delta^{12,14}$ Prostaglandin J_2 (15d-PGJ_2) is a metabolite of PGD_2, and is produced by mast cells, T cells, platelets and alveolar macrophages. 15d-PGJ_2 is recognized as an endogenous ligand for the intranuclear receptor PPARγ [13], which leads to inhibition of phorbol ester-induced nitric oxide and macrophage-derived

cytokines, i.e., tumor necrosis factor-α (TNF-α), IL-1 and IL-6. 15d-PGJ_2 inhibits gene expression in part by antagonizing the activities of transcription factors such as activator protein-1 and nuclear factor-κB (NF-κB) [7]. Furthermore, 15d-PGJ_2 has an anti-atherosclerotic effect as a ligand of PPARγ. Previous studies have been shown that 15d-PGJ_2 dose-dependently inhibits several functions of endothelial cells related to angiogenesis, such as proliferation, morphogenesis and migration in vitro [14–16]. Another study revealed that an increased plasma 15d-PGJ_2 concentration was associated with the early and late neurological outcomes, and a smaller infarct volume in ischemic stroke patients [17]. However, it remains unknown whether or not 15d-PGJ_2 has an anti-atherogenic effect in vivo. To investigate the effects of 15d-PGJ_2 on atherosclerotic lesion formation, we treated apo E–knockout mice, an animal model of atherosclerosis, with 15d-PGJ_2, and then examined the atherosclerotic lesions.

Methods

Animals

Apo E-knockout mice (C57BL/6J-Apoe^{tm1Unc}) were purchased from the Jackson Laboratory (B6 background; The Jackson Laboratory, Bar Habor, ME) [18]. These mice were produced by backcrossing the Apoe^{tm1Unc} mutation 10 times to C57BL/6J mice. Mice were maintained under specific pathogen-free conditions, and allowed ad libitum access to food and water. Thirty female animals aged 8 wk (15 as controls and 15 for the 15d-PGJ_2 experiments) were fed the Western-type diet containing 0.2% cholesterol and 21% saturated fat (Oriental Yeast, Tokyo, Japan) for 8 wk. All mice received intraperitoneal injections of (1) PBS (control group), and (2) 15d-PGJ_2 (Cayman Chemicals, Ann Arbor, USA), 1 mg/kg/day (15d-PGJ_2 group), for 8 wk with a high fat diet. Administration route and dosage of 15d-PGJ_2 were based on our previous study [19]. The animal care and experimental procedures conformed to the regulations of the Animal Research Committee, Graduate School of Medicine, Kyoto University.

Quantitative analyses of atherosclerotic lesions

Following blood collection, mice aged 16 wk treated with PBS or 15d-PGJ_2 were examined. After overnight fasting, blood was collected from the cardiac cavity and analyzed for the lipid profile. Also, aortae from the ascending portion to the end of the thoracic aorta were removed and washed meticulously in cold PBS to remove attached hematocytes and tissue fragments on the outside the aortae. Proximal aortic roots were used for quantitative analysis of the atherosclerotic area and whole thoracic aortae for real-time polymerase chain reaction (PCR) analysis.

Atherosclerotic lesions were quantitatively analyzed as previously described [20,21]. In brief, the basal portion of the heart and proximal aortic root were excised, embedded in OCT compound (Sakura Finetek, Tokyo, Japan), and then frozen in liquid nitrogen. Three serial cryosections per one aortic root of 10 μm thickness, at 40 μm intervals, of the aortic sinus were stained with oil-red O (Wako Pure Chemical Industries Ltd, Osaka, Japan) and hematoxylin. Other three cryosections per one aortic root were stained with Masson's trichrome (Kyodo Byori, Kobe, Japan) for cellular components (red) and fibrous tissue (blue). Lesion images were captured with a DMBA210 microscope (Shimadzu Rika, Tokyo, Japan) equipped with Motic Images Plus2.2s software (Shimadzu Rika, Tokyo, Japan). The captured images were analyzed with Image J software (NIH, USA). We calculated the oil-red O positive area, fibrotic area and aortic root area and compared the average data of three sections. A blind observer analyzed the lesions.

Immunohistochemistry

Immunohistochemistry was performed on 10 μm thick cryosections as described above. Tissue sections were immersed for 30 min in 0.3% hydrogen peroxide in methanol to block endogenous peroxidase activity. Nonspecific binding sites were saturated by exposure to 0.2% bovine serum albumin and normal serum for 30 min. Rat monoclonal anti-mouse macrophages (MOMA-2; AbD Serotec, Oxford, United Kingdom), goat anti-mouse monocyte chemoattractant protein-1 (MCP-1; Santa Cruz Biotechnology Inc., California, USA), rabbit anti-mouse macrophage migration inflammatory factor (MIF; Life Technologies, California, USA), goat anti-mouse TNF-α (R&D Systems, Minnesota, USA), goat anti-mouse matrix metallopeptidase-9 (MMP-9; Santa Cruz Biotechnology Inc., California, USA) and goat anti-mouse PPARγ (Santa Cruz Biotechnology Inc., California, USA) Abs were used as primary Abs. These primary anti-mouse macrophage Abs (1/50 dilution in PBS), anti-mouse MCP-1 Abs (1/100 dilution in PBS), anti-mouse MIF Abs (1/00 dilution in PBS), anti-mouse TNF-α Abs (1/100 dilution in PBS), anti-mouse MMP-9 Abs (1/100 dilution in PBS), anti-mouse PPARγ Abs (1/100 dilution in PBS) and control normal serum were applied to tissue sections, followed by incubation overnight at 4°C. The slides were treated with 0.2% glutaraldehyde. Then biotinylated secondary Abs and streptavidin–horseradish peroxidase were used for detection (Nichirei Bioscience, Tokyo, Japan) for 30 min. Signals were developed with a DAB Peroxidase Substrate Kit, 3,3′-diaminobenzidine (Vector Laboratories, Burlingame, USA). Positive staining was indicated by brownish black deposits, and counterstaining was performed with hematoxylin. The images were captured with a DMBA210 microscope, and the captured images were analyzed with Image J software (NIH, USA), the ratios of the positive area to the whole cross-sectional aortic wall area being calculated. Each data was average of three sections. A blind observer analyzed the lesions.

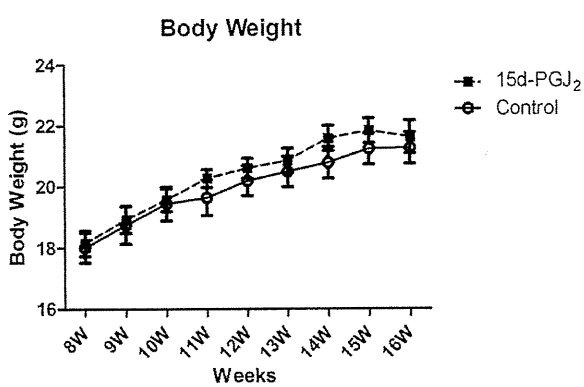

Figure 1. Body weights of apo E-knockout mice treated with PBS or 15d-PGJ_2 from 8 to 16 weeks of age. From the 8th week to 16th week, female mice were randomized to receive a Western-type diet and PBS or 1 mg/kg/day of 15d-PGJ_2 (n = 15 animals for each group). At 16th week, body weight of 15d-PGJ2 treated mice tended to be higher than controls, but it was not significantly different (21.6±4.2 g and 21.2±3.9 g, respectively, $p = 0.6$). Statistical analyses were performed with Student's t test.
doi:10.1371/journal.pone.0025541.g001

Real-time reverse-transcription polymerase chain reaction

Several gene expressions such as MCP-1, MIF, TNF-α, MMP-9 and RelA (p65), were analyzed by real-time quantitative RT-PCR using the TaqMan system based on real-time detection of accumulated fluorescence. Total RNA was extracted from whole thoracic aortae by homogenization in an RNeasy Fibrous Tissue Mini Kit (Qiagen Japan, Tokyo, Japan). cDNA was synthesized by reverse transcription with a Clontech Advantage RT-for-PCR Kit (Takara Bio Inc., Otsu, Japan). Quantitative real-time reverse-

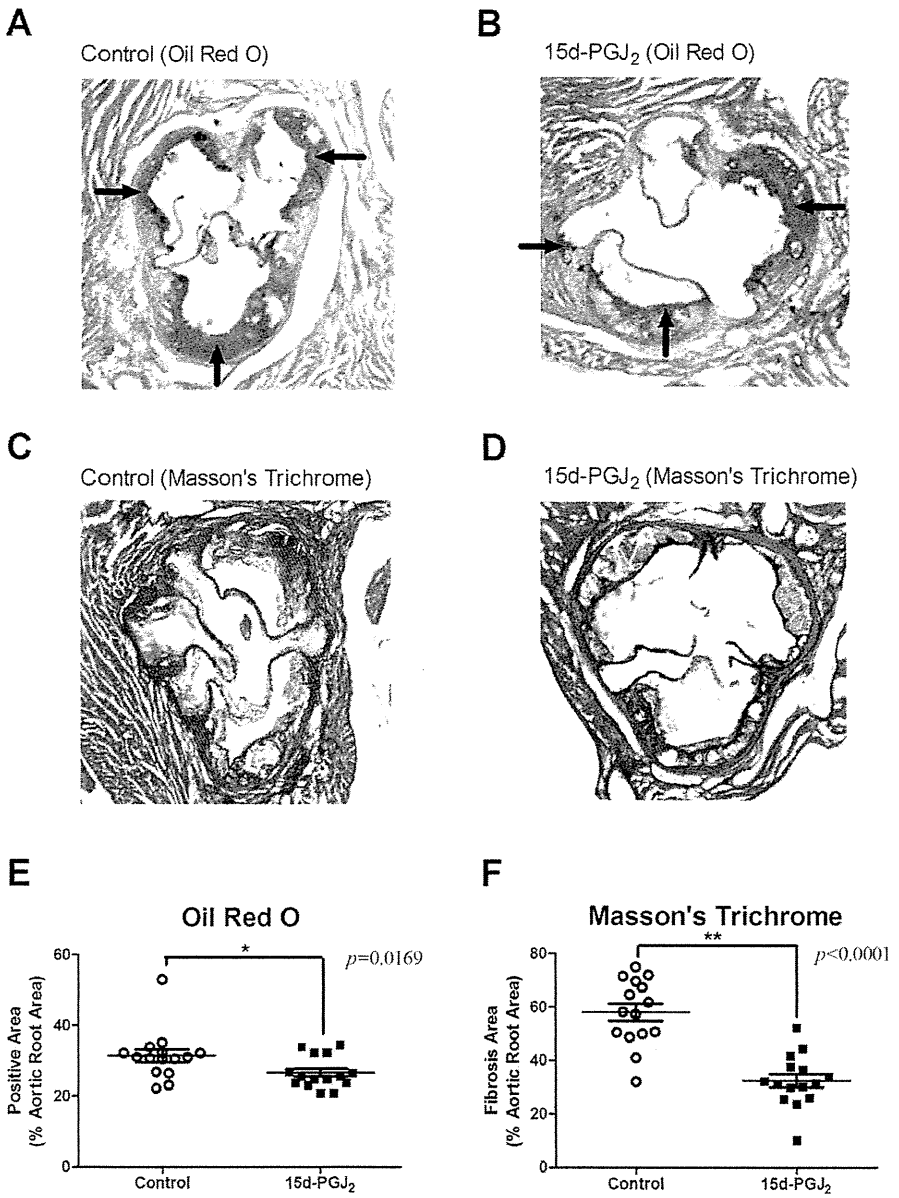

Figure 2. Representative oil red O stained sections and Masson's trichrome stained sections from the proximal aortae of apo E-knockout mice, and prevalence of atherosclerotic lesions. A and B are representative oil red O stained sections from the proximal aortae of apo E-knockout mice. C and D are representative Masson's trichrome stained sections. Apo E knockout-mice were fed a Western-type diet and treated with PBS (control group) (n = 15) (A, C) or 1 mg/kg/day 15d-PGJ_2 (15d-PGJ_2 group) (n = 15) (B, D) for 2 mo. Cross-sections of proximal aortae were stained with oil red O and counterstained with hematoxylin. Black arrows indicate the positive lesions. We plotted the prevalence of oil red O positive areas in cross-sections of whole atherosclerotic lesions in each group (E). Short lines indicate the means ± SD. The prevalence in controls were 31.44±1.811% and 26.63±1.169%, respectively. Cross-sections of proximal aortae were also stained with Masson's trichrome for cellular components (smooth muscle cells: pink, and red blood cells: red) and fibrous tissue (blue). We plotted the prevalence of fibrosis areas in cross-sections of whole atherosclerotic lesions in each group (F). Short lines indicate the means ± SD. The prevalence of fibrotic areas in controls were 58.05±3.218% and 32.48±2.535%, respectively. Statistical analyses were performed with Student's t test. *$p<0.05$, **$p<0.01$.
doi:10.1371/journal.pone.0025541.g002

transcription polymerase chain reaction was performed using an Applied Biosystems 7300 Real-Time PCR System (Applied Biosystems, California, USA), followed by analysis involving software detection system (SDS version 1.9) software. Gene expression was normalized as to 18S rRNA (Applied Biosystems).

Lipid metabolism

After overnight fasting, blood was collected from the cardiac cavity of mice aged 16 wk and analyzed for the lipid profile. The plasma chylomicron (CM), very low density lipoprotein (VLDL), low density lipoprotein (LDL), and high density lipoprotein (HDL) levels were determined by use of a high-sensitivity lipoprotein-profiling system by high-performance liquid chromatography (HPLC) (Skylight Biotech, Inc., Akita, Japan) [22]. HPLC with gel permeation columns was performed to classify and quantify lipoproteins on the basis of differences in particle size [23].

Statistical analysis

The results were expressed as means ± SE and analyzed by means of Student's t test (GraphPad Prism 5.03; Graph Pad Software Inc., CA, USA). Values of $p<0.05$ were considered statistically significant.

Results

Body weight

From the 8th week to 16th week, mice were randomized to receive a Western-type diet and PBS or 15d-PGJ_2. Figure 1 shows the change of body weight for observation period. At 16th week, body weight of 15d-PGJ_2 treated mice tended to be higher than controls, but it was not significantly different (21.6±4.2 g and 21.2±3.9 g, respectively, $p=0.6$). Body weight did not decrease after intraperitoneal administration of PBS or 15d-PGJ_2.

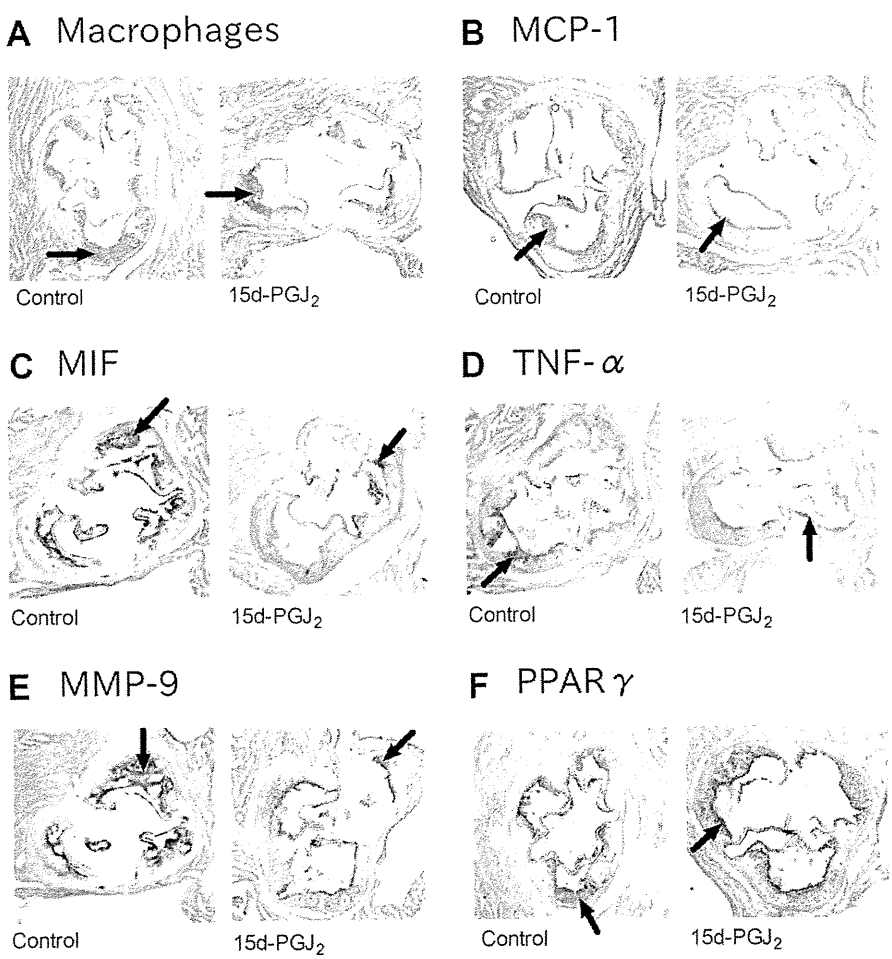

Figure 3. Representative sections with immunohistochemical analysis. Apo E-knockout mice were fed a Western-type diet and treated with PBS (control group) (n=10) or 1 mg/kg/day 15d-PGJ_2 (15d-PGJ_2 group) (n=10) for 2 mo. Representative cross-sections of the aortic sinus were stained with MOMA-2 (A), which detected macrophages, and MCP-1 Abs (B), MIF Abs (C), TNF-α Abs (D), MMP-9 Abs (E), PPARγ Abs (F), and counterstained with hematoxylin. Right sections are control group and left ones are 15d-PGJ_2 group in each figure. Black arrows indicate the positive lesions.
doi:10.1371/journal.pone.0025541.g003

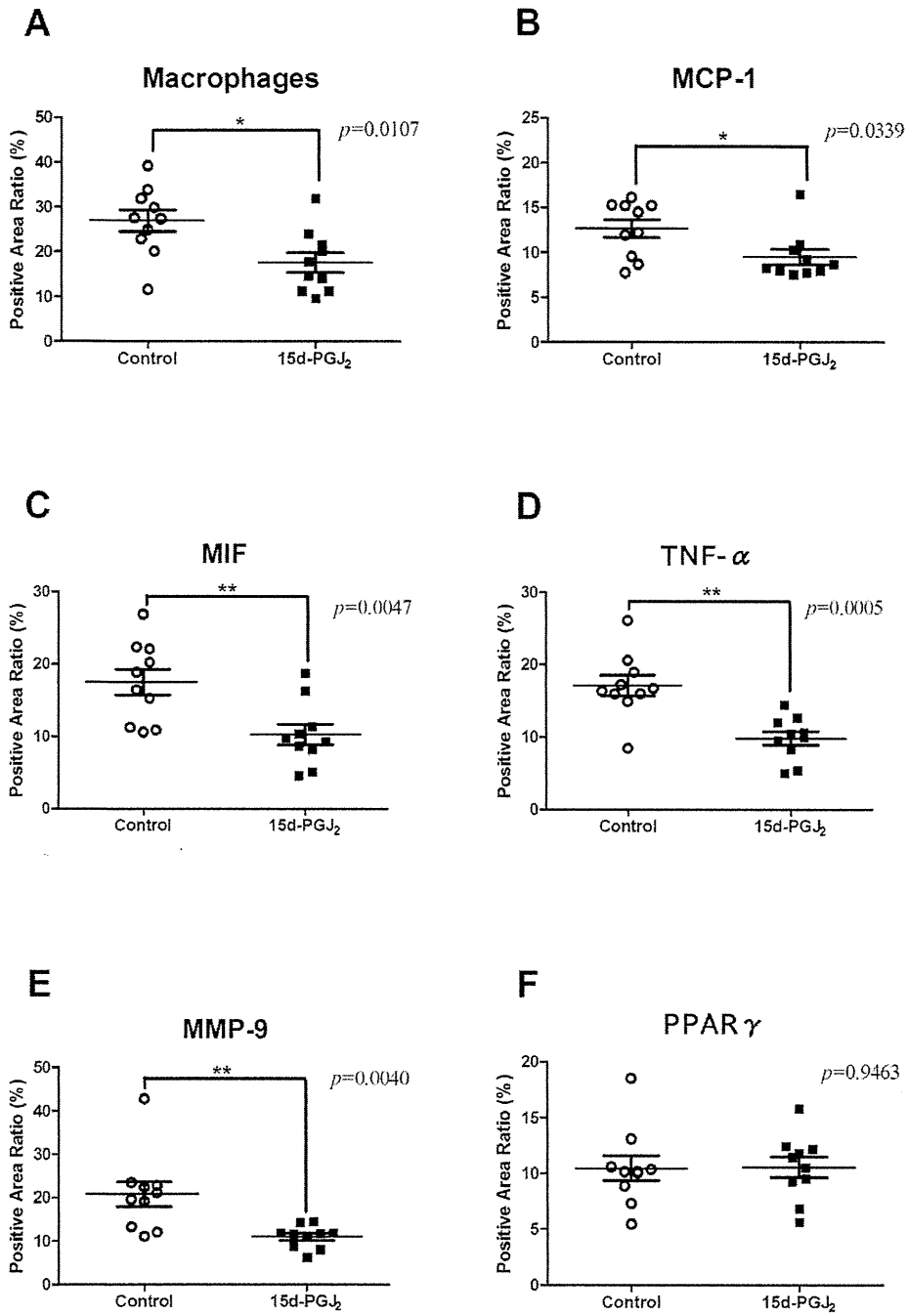

Figure 4. Prevalence of atherosclerotic lesions with immunohistochemical analysis. Apo E-knockout mice were fed a Western-type diet and treated with PBS (control group) (n = 10) or 1 mg/kg/day 15d-PGJ_2 (15d-PGJ_2 group) (n = 10) for 2 mo. Representative cross-sections of the aortic sinus were stained with MOMA-2, which detected macrophages, and MCP-1 Abs, MIF Abs, TNF-α Abs, MMP-9 Abs, PPARγ Abs, and counterstained with hematoxylin. We plotted the prevalence of positive areas in cross-sections of whole atherosclerotic lesions in each group. Short lines indicate the means ± SD. The prevalence of macrophage (A), immunoreactive MCP-1 (B), MIF (C), TNF-α (D) and MMP-9 (E) in atherosclerotic lesions of apo E-knockout mice treated with PBS or 15d-PGJ2 was examined. The prevalence of macrophage in the control and 15d-PGJ_2 groups were 26.97±2.437% and 17.64±2.194%, respectively. The prevalence of immunoreactive MCP-1 (9.508±0.8518% vs 12.65±0.9788%, $p = 0.0339$), MIF (10.28±1.402% vs 17.53±1.762%, $p = 0.0047$), TNF-α (9.853±0.9462% vs 17.12±1.412%, $p = 0.0005$) and MMP-9 (11.02±0.8208% vs 20.80±2.846%, $p = 0.0040$) were decreased in the 15d-PGJ_2 groups. But the prevalence of PPARγ (F) was not different between both groups (10.55±0.9217% vs 10.46±1.104%, $p = 0.9463$). *$p<0.05$, **$p<0.01$, with Student's t test.
doi:10.1371/journal.pone.0025541.g004

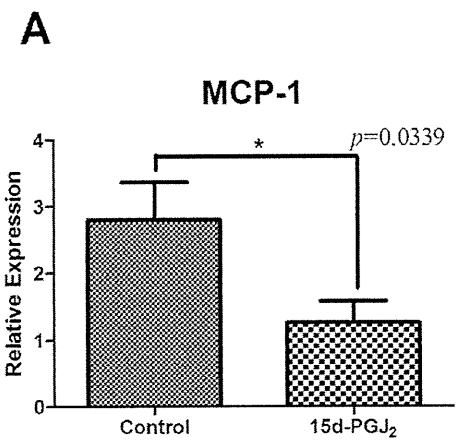
A
MCP-1
Relative Expression
*
p=0.0339
Control
15d-PGJ2

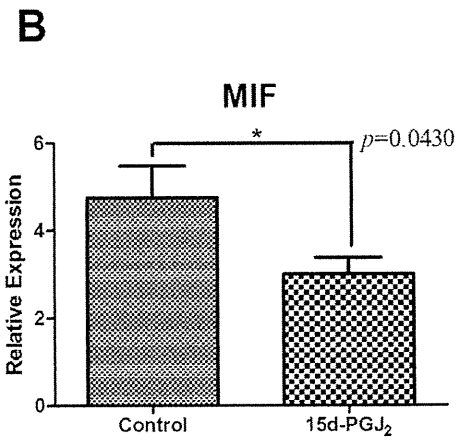
B
MIF
Relative Expression
*
p=0.0430
Control
15d-PGJ2

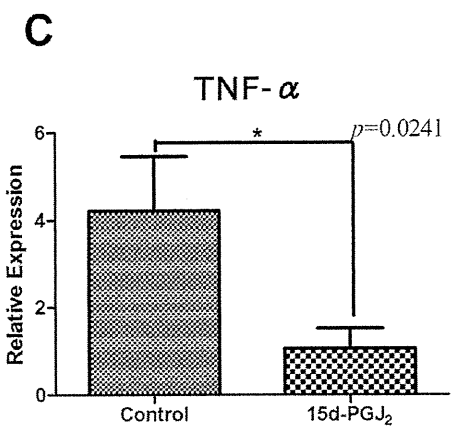
C
TNF-α
Relative Expression
*
p=0.0241
Control
15d-PGJ2

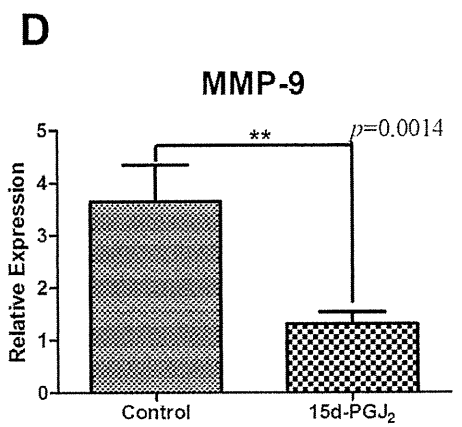
D
MMP-9
Relative Expression
**
p=0.0014
Control
15d-PGJ2

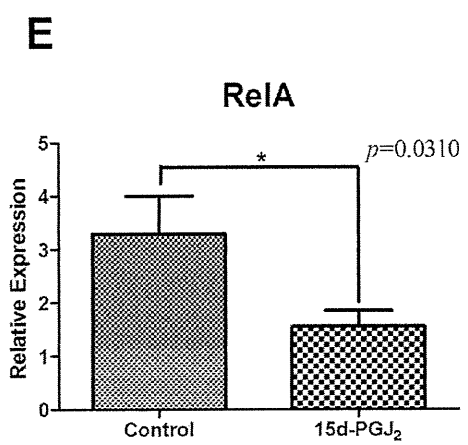
E
RelA
Relative Expression
*
p=0.0310
Control
15d-PGJ2

Figure 5. Comparison of gene expressions in the thoracic aorta between the control and 15d-PGJ_2 treated groups by real-time PCR analysis. Apo E-knockout mice were fed a Western-type diet and treated with PBS (control group) or 1 mg/kg/day 15d-PGJ_2 (15d-PGJ_2 group) for 2 mo. Thoracic aortae were removed and total RNA was extracted from them. cDNA was synthesized by reverse transcription, and quantitative real-time PCR was performed. The relative gene expression values were calculated. The relative expressions were significantly decreased in the 15d-PGJ_2 group, MCP-1 (1.263±0.3193 vs 2.802±0.5627, $p=0.0339$) (A), MIF (2.985±0.3860 vs 4.745±0.7347, $p=0.0430$) (B), TNF-α (1.059±0.4625 vs 4.220±1.236, $p=0.0241$) (C), MMP-9 (1.304±0.2344 vs 3.644±0.6947, $p=0.0014$) (D) and RelA (1.551±0.2995 vs 3.294±0.7093, $p=0.0310$) (E), compared with in the control group. *$p<0.05$, **$p<0.01$, with Student's t test.
doi:10.1371/journal.pone.0025541.g005

Atherosclerotic lesions in the aortic sinus

To determine the factors mediating the anti-atherosclerotic effect of 15d-PGJ_2, we compared the area of oil red O-positive lesions and fibrotic lesions in cross-sections of the aortic wall between the control and 15d-PGJ_2 groups (n = 15, respectively). Representative micrographs are presented in Figure 2. Typical atheromas with well-developed, lipid-rich cores and foam cell infiltration were observed. The prevalence of oil red O positive areas in cross-sections of whole atherosclerotic lesions were 31.44±1.811% in the controls and 26.63±1.169% in the 15d-PGJ_2 groups. The prevalence of Masson's trichrome stained fibrotic areas were 58.05±3.218% and 32.48±2.535%, respectively.

Immunohistochemistry of the atherosclerotic lesions

We explored the mechanism underlying the anti-atherosclerotic effect of 15d-PGJ_2. Immunohistochemistry was performed with MOMA-2, which detected macrophages, anti-MCP-1 Abs, anti-MIF Abs, anti- TNF-α Abs, and anti-MMP-9 Abs. We compared the prevalence of positive areas in the aortic root between the control and 15d-PGJ_2 groups (n = 10, respectively). The 15d-PGJ_2 group exhibited significant lower expression of MCP-1 (9.508±0.8518% vs 12.65±0.9788%, $p=0.0339$), MIF (10.28±1.402% vs 17.53±1.762%, $p=0.0047$), TNF-α (9.853±0.9462% vs 17.12±1.412%, $p=0.0005$), MMP-9 (11.02±0.8208% vs 20.80±2.846%, $p=0.0040$) and macrophages (17.64±2.194% vs 26.97±2.437%, $p=0.0107$), compared with in control group (Figure 3A–3E, Figure 4A–4E). But the prevalence of PPARγ was not different between both groups (10.55±0.9217% vs 10.46±1.104%, $p=0.9463$) (Figure 3F, Figure 4F).

Gene expressions in the thoracic aorta

Figure 5 shows the results of quantitative real-time PCR analysis of MCP-1, MIF, TNFα, MMP-9 and RelA gene expressions in thoracic aortae. All of those gene expressions were significantly decreased in the 15d-PGJ_2 group (n = 10, respectively), MCP-1 (1.263±0.3193 vs 2.802±0.5627, $p=0.0339$), MIF (2.985±0.3860 vs 4.745±0.7347, $p=0.0430$), TNF-α (1.059±0.4625 vs 4.220±1.236, $p=0.0241$), MMP-9 (1.304±0.2344 vs 3.644±0.6947, $p=0.0014$) and RelA (1.551±0.2995 vs 3.294±0.7093, $p=0.0310$), compared with in the control group. 15d-PGJ_2 also reduced the expressions of these atherosclerotic markers at the gene level. It indicated that 15d-PGJ_2 led to downregulation of these gene expressions via NF-κB, and these results were almost comparable with immunohistochemistry. In addition, ligand-induced negative-feedback was not identified in our study.

15d-PGJ_2 treatment improves the lipid profile

We performed analyses of lipid levels at the end of this study. Pooled plasma from all mice was subjected to HPLC. Lipoproteins were separated in CM, VLDL, LDL, and HDL. The total serum cholesterol level was significantly lower in the15d-PGJ_2 group than in the control group (795.5±39.31 mg/dl vs 944.1±49.04 mg/dl, $p=0.029$) (Figure 6A). Especially LDL was significantly reduced in the 15d-PGJ_2 group (186.9±13.49 mg/dl vs 234.3±16.60 mg/dl, $p=0.0397$) (Figure 6D). CM and VLDL tended to be lower than in controls, but the difference was not significant (36.96±4.999 mg/dl vs 68.13±23.98 mg/dl, p = 0.1415; 553.5±26.67 mg/dl vs 622.7±28.02 mg/dl, $p=0.1005$, respectively) (Figure 6B and C). The HDL level was not different between the control and 15d-PGJ_2 groups (18.14±1.264 mg/dl vs 19.01±2.562 mg/dl, $p=0.7413$) (Figure 6E).

Discussion

15d-PGJ_2 is a ligand of PPARγ, which acts to atherosclerosis formation. In this study, we fed apo E-deficient mice a Western-type diet and administered 15d-PGJ_2. We measured the cross-sectional atherosclerotic area in the proximal aorta and examined the expression of several atherosclerotic markers in the lesions. The atherosclerotic area, represented by lipid accumulation and fibrous tissue, significantly decreased in apo E-null mice treated with 15d-PGJ_2. Immunohistochemical and real-time PCR analyses showed that the expressions of MCP-1, MIF, TNF-α and MMP-9 in atherosclerotic lesions were significantly decreased. The 15d-PGJ_2 also reduced the expression of RelA mRNA in atherosclerotic lesions. This study suggests that 15d-PGJ_2 has an anti-atherosclerotic effect.

Atherosclerosis is an inflammatory disease. The lesions in atherosclerosis represent a series of highly specific cellular and molecular responses that can best be described, overall, as an inflammatory disease [24]. Atherosclerosis formation consists of several steps. The earliest changes that precede the formation of lesions of atherosclerosis take place in the endothelium. These changes include migration of leukocytes into the artery wall, which is mediated by MCP-1 [24]. Fatty streaks initially consist of lipid-laden monocytes and macrophages together with T lymphocytes. Later they are joined by various numbers of smooth-muscle cells. The steps involved in this process include T cell activation, foam-cell formation, which is mediated by TNF-α. As the advanced change, thinning of the fibrous cap is apparently due to the continuing influx and activation of macrophages, which release metalloproteinases such as MMP-9, and other proteolytic enzymes at these sites. MIF affects cell proliferation in lesions and elastolytic/collagenolytic cysteine protease expression. MIF may act as do other cytokines (eg, TNF-α) to enhance protease expression and vascular cell proliferation, processes that occur during atherogenesis [25]. Our data showed that 15d-PGJ_2 inhibited MCP-1, MIF, TNF-α and MMP-9 as indicated by real-time PCR as well as immunohistochemical analysis. A previous study showed that thiazolidinediones and 15d-PGJ_2 inhibit macrophage proliferation in a dose-dependent manner, and significantly reduce the migration of monocytes induced by MCP-1 in vitro [26]. Also, MCP-1 is one of the important mediators at early change of atherosclerosis formation. On possibility is that 15d-PGJ_2 act on various steps of atherosclerosis formation. Another possibility is that 15d-PGJ_2 act on the early step of atherosclerosis formation, as a consequence, 15d-PGJ_2 decrease the mediators at following steps.

15d-PGJ_2 is one of the PPARγ-ligands [13] emerging as a key anti-inflammatory mediator via NF-κB inhibition, may play a role in the pathogenesis of atherosclerosis [2]. NF-κB family consists of

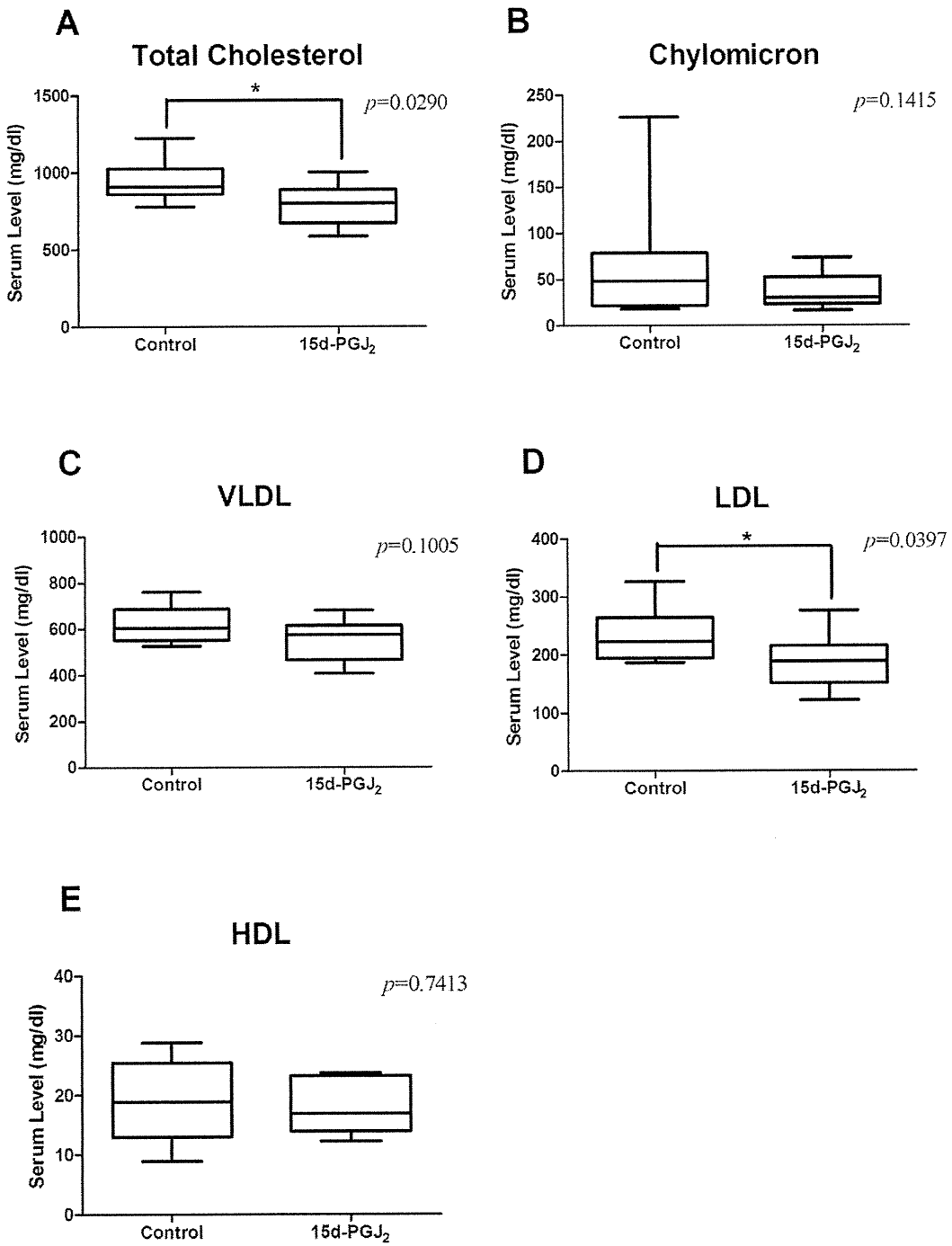

Figure 6. Serum lipid levels in the controls and the 15d-PGJ_2 group. Blood was collected from the cardiac cavity of mice aged 16 wk and analyzed for the lipid profile. The plasma chylomicron (CM) (B), very low density lipoprotein (VLDL) (C), low density lipoprotein (LDL) (D), and high density lipoprotein (HDL) (E) levels were determined by use of a high-sensitivity lipoprotein-profiling system by high-performance liquid chromatography. The total serum cholesterol level (A) was significantly lower in the15d-PGJ_2 group than in the control group (795.5±39.31 mg/dl vs 944.1±49.04 mg/dl, $p=0.029$). Especially LDL was significantly reduced in the 15d-PGJ_2 group (186.9±13.49 mg/dl vs 234.3±16.60 mg/dl, $p=0.0397$). CM, VLDL and HDL were not different between the control and 15d-PGJ_2 groups, 36.96±4.999 mg/dl vs 68.13±23.98 mg/dl, 553.5±26.67 mg/dl vs 622.7±28.02 mg/dl, 18.14±1.264 mg/dl vs 19.01±2.562 mg/dl, respectively. *$p<0.05$, with Student's t test.
doi:10.1371/journal.pone.0025541.g006

RelA (p65), c-Rel, and RelB, as well as p105 and p100 and their processed forms, p50 and p52, respectively. NF-κB primarily exists as a p50/p65 heterodimer [27]. In our data, PPARγ expressed in atherosclerotic lesions in both controls and 15d-PGJ_2 groups. In addition, the expression of RelA was decreased in 15d-PGJ_2 groups. It is generally known that high dose of ligands lead to downregulation of its receptor expressions. Although it has not been reported about PPARγ agonist, a previous study revealed that treatment with GW1929, a selective PPARγ antagonist, enhanced PPARγ mRNA expressions in kidneys from hypertension model rats [28]. This study shows the possibility that high dose PPARγ also downregulate its receptor expression. But PPARγ expression was not changed in our results. It indicated that 15d-PGJ_2 did not induce the negative-feedback in our study. On the other hand, the reduction of RelA was owing to NF-κB inhibition. 15d-PGJ_2 induces some PPARγ-independent biological actions, such as inhibition of NF-κB signaling through covalent modifications of critical cysteine residues in IκB kinase and the DNA-binding domains of NF-κB subunits [29]. We presumed that 15d-PGJ_2 inhibited NF-κB not only as a PPARγ agonist but also as PPARγ-independent actions.

High plasma concentrations of cholesterol, in particular those of LDL cholesterol, are one of the principal risk factors for atherosclerosis [24]. In this study, 15d-PGJ_2 decreased serum total cholesterol level and LDL cholesterol level. This shows that 15d-PGJ_2 reduces the principal risk factor of atherosclerosis. But the detail mechanisms remain an open question. Further studies are needed to elucidate this matter.

In conclusion, this is the first study demonstrating an anti-atherosclerotic effect of 15d-PGJ_2 in vivo, using a rodent model. The mechanism of its effect remains to be elucidated in detail. However, our data indicate that 15d-PGJ_2 exhibits ability as to an anti-atherosclerotic effect. These findings suggest that 15d-PGJ_2 is a beneficial therapeutic reagent for both atherosclerosis.

Acknowledgments

We would like to thank Saori Bessho for helpful assistance during these studies.

Author Contributions

Conceived and designed the experiments: TS MH MK YK. Performed the experiments: TS MH AY MK KN. Analyzed the data: TS MH. Contributed reagents/materials/analysis tools: TS MH EA HI AY MK KM. Wrote the paper: TS MK SM YK. Assisted editing paper: EA MK SM TM YK.

References

1. Libby P, Ridker PM (2006) Inflammation and Atherothrombosis From Population Biology and Bench Research to Clinical Practice. Journal of the American College of Cardiology 48: A33–A46. Available: http://linkinghub.elsevier.com/retrieve/pii/S0735109706019966. Accessed 23 Jul 2010.
2. Ricote M, Huang J, Fajas L, Li A, Welch J, et al. (1998) Expression of the peroxisome proliferator-activated receptor gamma (PPARgamma) in human atherosclerosis and regulation in macrophages by colony stimulating factors and oxidized low density lipoprotein. Proceedings of the National Academy of Sciences of the United States of America 95: 7614–9. Available: http://www.pubmedcentral.nih.gov/articlerender.fcgi?artid = 22700&tool = pmcentrez&rendertype = abstract. Accessed 31 Aug 2010.
3. Chen Z, Ishibashi S, Perrey S, Osuga Ji, Gotoda T, et al. (2001) Troglitazone inhibits atherosclerosis in apolipoprotein E-knockout mice: pleiotropic effects on CD36 expression and HDL. Arteriosclerosis, thrombosis, and vascular biology 21: 372–7. Available: http://www.ncbi.nlm.nih.gov/pubmed/11231916.
4. Shinohara E, Kihara S, Ouchi N, Funahashi T, Nakamura T, et al. (1998) Troglitazone suppresses intimal formation following balloon injury in insulin-resistant Zucker fatty rats. Atherosclerosis 136: 275–9. Available: http://www.ncbi.nlm.nih.gov/pubmed/9543098. Accessed 14 Oct 2010.
5. Jiang C, Ting AT, Seed B (1998) PPAR-gamma agonists inhibit production of monocyte inflammatory cytokines. Nature 391: 82–6. Available: http://www.ncbi.nlm.nih.gov/pubmed/9422509. Accessed 31 Aug 2010.
6. Toriumi Y, Hiraoka M, Watanabe M, Yoshida M (2003) Pioglitazone reduces monocyte adhesion to vascular endothelium under flow by modulating RhoA GTPase and focal adhesion kinase. FEBS letters 553: 419–22. Available: http://www.ncbi.nlm.nih.gov/pubmed/14572662. Accessed 21 Jul 2010.
7. Ricote M, Li AC, Willson TM, Kelly CJ, Glass CK (1998) The peroxisome proliferator-activated receptor-gamma is a negative regulator of macrophage activation. Nature 391: 79–82. Available: http://www.ncbi.nlm.nih.gov/pubmed/9422508.
8. Bonfield TL, Thomassen MJ, Farver CF, Abraham S, Koloze MT, et al. (2008) Peroxisome proliferator-activated receptor-gamma regulates the expression of alveolar macrophage macrophage colony-stimulating factor. Journal of immunology (Baltimore, Md. : 1950) 181: 235–42. Available: http://www.pubmedcentral.nih.gov/articlerender.fcgi?artid = 2819287&tool = pmcentrez&rendertype = abstract. Accessed 22 Oct 2010.
9. Zhang W-Y, Schwartz EA, Permana PA, Reaven PD (2008) Pioglitazone inhibits the expression of inflammatory cytokines from both monocytes and lymphocytes in patients with impaired glucose tolerance. Arteriosclerosis, thrombosis, and vascular biology 28: 2312–8. Available: http://www.ncbi.nlm.nih.gov/pubmed/18818415. Accessed 22 Oct 2010.
10. Jackson SM, Parhami F, Xi XP, Berliner JA, Hsueh WA, et al. (1999) Peroxisome proliferator-activated receptor activators target human endothelial cells to inhibit leukocyte-endothelial cell interaction. Arteriosclerosis, thrombosis, and vascular biology 19: 2094–104. Available: http://www.ncbi.nlm.nih.gov/pubmed/10479650.
11. Pasceri V, Wu HD, Willerson JT, Yeh ET (2000) Modulation of vascular inflammation in vitro and in vivo by peroxisome proliferator-activated receptor-gamma activators. Circulation 101: 235–8. Available: http://www.ncbi.nlm.nih.gov/pubmed/10645917.
12. Harris SG, Padilla J, Koumas L, Ray D, Phipps RP (2002) Prostaglandins as modulators of immunity. Trends in immunology 23: 144–50. Available: http://www.ncbi.nlm.nih.gov/pubmed/11864843.
13. Ide T, Egan K, Bell-Parikh LC, FitzGerald GA (2003) Activation of nuclear receptors by prostaglandins. Thrombosis research 110: 311–5. Available: http://www.ncbi.nlm.nih.gov/pubmed/14592554. Accessed 14 Oct 2010.
14. Bishop-Bailey D, Hla T (1999) Endothelial cell apoptosis induced by the peroxisome proliferator-activated receptor (PPAR) ligand 15-deoxy-Delta12, 14-prostaglandin J2. The Journal of biological chemistry 274: 17042–8. Available: http://www.ncbi.nlm.nih.gov/pubmed/10358055.
15. Xin X, Yang S, Kowalski J, Gerritsen ME (1999) Peroxisome proliferator-activated receptor gamma ligands are potent inhibitors of angiogenesis in vitro and in vivo. The Journal of biological chemistry 274: 9116–21. Available: http://www.ncbi.nlm.nih.gov/pubmed/10085162.
16. Dong Y-G, Chen D-D, He J-G, Guan Y-Y (2004) Effects of 15-deoxy-delta12,14-prostaglandin J2 on cell proliferation and apoptosis in ECV304 endothelial cells. Acta pharmacologica Sinica 25: 47–53. Available: http://www.ncbi.nlm.nih.gov/pubmed/14704122.
17. Blanco M, Moro MA, Dávalos A, Leira R, Castellanos M, et al. (2005) Increased plasma levels of 15-deoxyDelta prostaglandin J2 are associated with good outcome in acute atherothrombotic ischemic stroke. Stroke; a journal of cerebral circulation 36: 1189–94. Available: http://www.ncbi.nlm.nih.gov/pubmed/15879329. Accessed 22 Oct 2010.
18. Piedrahita JA, Zhang SH, Hagaman JR, Oliver PM, Maeda N (1992) Generation of mice carrying a mutant apolipoprotein E gene inactivated by gene targeting in embryonic stem cells. Proceedings of the National Academy of Sciences of the United States of America 89: 4471–5. Available: http://www.pubmedcentral.nih.gov/articlerender.fcgi?artid = 49104&tool = pmcentrez&rendertype = abstract.
19. Kawahito Y, Kondo M, Tsubouchi Y, Hashiramoto A, Bishop-Bailey D, et al. (2000) 15-deoxy-delta(12,14)-PGJ(2) induces synoviocyte apoptosis and suppresses adjuvant-induced arthritis in rats. The Journal of clinical investigation 106: 189–97. Available: http://www.pubmedcentral.nih.gov/articlerender.fcgi?artid = 314310&tool = pmcentrez&rendertype = abstract. Accessed 13 Jul 2010.
20. Hamaguchi M, Seno T, Yamamoto A, Kohno M, Kadoya M, et al. (2010) Loxoprofen Sodium, a Non-Selective NSAID, Reduces Atherosclerosis in Mice by Reducing Inflammation. Journal of Clinical Biochemistry and Nutrition 47: 138–147. Available: http://joi.jlc.jst.go.jp/JST.JSTAGE/jcbn/10-33?from = CrossRef.
21. Paigen B, Morrow A, Holmes PA, Mitchell D, Williams RA (1987) Quantitative assessment of atherosclerotic lesions in mice. Atherosclerosis 68: 231–240. Available: http://www.ncbi.nlm.nih.gov/entrez/query.fcgi?cmd = Retrieve&db = PubMed&dopt = Citation&list_uids = 3426656.
22. Usui S, Hara Y, Hosaki S, Okazaki M (2002) A new on-line dual enzymatic method for simultaneous quantification of cholesterol and triglycerides in lipoproteins by HPLC. Journal of lipid research 43: 805–14. Available: http://www.ncbi.nlm.nih.gov/pubmed/11971952.
23. Okazaki M, Usui S, Ishigami M, Sakai N, Nakamura T, et al. (2005) Identification of unique lipoprotein subclasses for visceral obesity by component

analysis of cholesterol profile in high-performance liquid chromatography. Arteriosclerosis, thrombosis, and vascular biology 25: 578–84. Available: http://www.ncbi.nlm.nih.gov/pubmed/15637308. Accessed 16 Oct 2010.

24. Ross R (1999) Atherosclerosis–an inflammatory disease. The New England journal of medicine 340: 115–26. Available: http://www.ncbi.nlm.nih.gov/pubmed/9887164.
25. Pan J-H, Sukhova GK, Yang J-T, Wang B, Xie T, et al. (2004) Macrophage migration inhibitory factor deficiency impairs atherosclerosis in low-density lipoprotein receptor-deficient mice. Circulation 109: 3149–53. Available: http://www.ncbi.nlm.nih.gov/pubmed/15197138. Accessed 6 Jul 2011.
26. Tanaka T, Fukunaga Y, Itoh H, Doi K, Yamashita J, et al. (2005) Therapeutic potential of thiazolidinediones in activation of peroxisome proliferator-activated receptor gamma for monocyte recruitment and endothelial regeneration. European journal of pharmacology 508: 255–65. Available: http://www.ncbi.nlm.nih.gov/pubmed/15680279. Accessed 10 Sep 2010.
27. Ghosh S, Karin M (2002) Missing pieces in the NF-kappaB puzzle. Cell 109 Suppl: S81–96. Available: http://www.ncbi.nlm.nih.gov/pubmed/11983155. Accessed 6 Sep 2010.
28. Yousefipour Z, Oyekan A, Newaz M (2009) Role of G protein-coupled receptor kinase-2 in peroxisome proliferator-activated receptor gamma-mediated modulation of blood pressure and renal vascular reactivity in SHR. American journal of nephrology 30: 201–8. doi:10.1159/000218061.
29. Straus DS, Pascual G, Li M, Welch JS, Ricote M, et al. (2000) 15-deoxy-delta 12,14-prostaglandin J2 inhibits multiple steps in the NF-kappa B signaling pathway. Proceedings of the National Academy of Sciences of the United States of America 97: 4844–9. Available: http://www.pubmedcentral.nih.gov/articlerender.fcgi?artid = 18320&tool = pmcentrez&rendertype = abstract. Accessed 7 Aug 2011.

Galectin-3 (Gal-3) induced by leukemia microenvironment promotes drug resistance and bone marrow lodgment in chronic myelogenous leukemia

Mio Yamamoto-Sugitani[a,b], Junya Kuroda[a,b,1], Eishi Ashihara[c], Hisao Nagoshi[a,b], Tsutomu Kobayashi[a,b], Yosuke Matsumoto[a,b], Nana Sasaki[a,b], Yuji Shimura[a,b], Miki Kiyota[a,b], Ryuko Nakayama[a,b], Kenichi Akaji[d], Tomohiko Taki[e], Nobuhiko Uoshima[f], Yutaka Kobayashi[g], Shigeo Horiike[a,b], Taira Maekawa[h], and Masafumi Taniwaki[a,b]

[a]Division of Hematology and Oncology, Department of Medicine, Kyoto Prefectural University of Medicine, Kyoto 602-8566, Japan; Departments of [b]Molecular Hematology and Oncology, [c]Molecular Cell Physiology, [d]Chemistry, and [e]Molecular Diagnostics and Therapeutics, Graduate School of Medical Science, Kyoto Prefectural University of Medicine, Kyoto 602-8566, Japan; [f]Department of Hematology, Matsushita Memorial Hospital, Osaka 570-8540, Japan; [g]Department of Hematology, Kyoto Second Red Cross Hospital, Kyoto 602-8026, Japan; and [h]Department of Transfusion Medicine and Cell Therapy, Kyoto University Hospital, Kyoto 606-8507, Japan

Edited* by Suzanne Cory, Walter and Eliza Hall Institute, Melbourne, Australia, and approved September 19, 2011 (received for review July 12, 2011)

Bone marrow (BM) microenvironment (BMME) constitutes the sanctuary for leukemic cells. In this study, we investigated the molecular mechanisms for BMME-mediated drug resistance and BM lodgment in chronic myelogenous leukemia (CML). Gene-expression profile as well as signal pathway and protein analyses revealed that galectin-3 (Gal-3), a member of the β-gal–binding galectin family of proteins, was specifically induced by coculture with HS-5 cells, a BM stroma cell-derived cell line, in all five CML cell lines examined. It was also found that primary CML cells expressed high levels of Gal-3 in BM. Enforced expression of Gal-3 activated Akt and Erk, induced accumulation of Mcl-1, and promoted in vitro cell proliferation, multidrug resistance to tyrosine kinase inhibitors for Bcr-Abl and genotoxic agents as a result of impaired apoptosis induction, and chemotactic cell migration to HS-5–derived soluble factors in CML cell lines independently of Bcr-Abl tyrosine kinase. The conditioned medium from Gal-3–overexpressing CML cells promoted in vitro cell proliferation of CML cells and HS-5 cells more than did the conditioned medium from parental cells. Moreover, the in vivo study in a mice transplantation model showed that Gal-3 overexpression promoted the long-term BM lodgment of CML cells. These results demonstrate that leukemia microenvironment-specific Gal-3 expression supports molecular signaling pathways for disease maintenance in BM and resistance to therapy in CML. They also suggest that Gal-3 may be a candidate therapeutic target to help overcome BMME-mediated therapeutic resistance.

Philadelphia-positive leukemia | bone marrow niche | chemoresistance | minimal residual disease

Chronic myelogenous leukemia (CML) is characterized by Bcr-Abl fusion tyrosine kinase (TK) as a result of the Philadelphia chromosome (Ph). Major advances in the treatment of CML have resulted from molecularly targeted therapeutic agents, such as imatinib mesylate (IM), which is the first-in-class Bcr-Abl TK inhibitor (TKI) and the more potent second-generation TKIs, such as nilotinib and dasatinib (Das) (1, 2). However, the complete elimination of CML clones has rarely been achieved by TKIs because of a variety of cell-intrinsic and cell-extrinsic protective mechanisms. The former include Bcr-Abl–related mechanisms, such as point mutations in the Abl kinase domain, and a variety of molecular abnormalities unrelated to Bcr-Abl (3–9). The latter include support of the bone marrow (BM) microenvironment (BMME), the so-called leukemia niche, which consists of soluble factors and supporting tissues, such as BM stromal cells (BMSCs), extracellular matrix (ECM), or hypoxia (10–19). Various new agents have been proposed for overcoming cell-intrinsic mechanisms for drug resistance (20, 21), and the precise molecular mechanisms for CML cell protection and maintenance by BMME sanctuary are not yet fully understood.

With the aim of developing new therapeutic strategies to overcome BMME-mediated protection of CML cells, we investigated the molecular mechanisms regulated by BMME, e.g., BMSCs and ECM, which enable leukemic cells to reside in the BM niche. Our study identified the involvement of galectin-3 (Gal-3), a member of the β-gal–binding galectin family of proteins, in BMME-mediated cell proliferation, protection, and BM lodgment. Gal-3 associates with cell proliferation, migration, adhesion, and apoptosis (22–26), and moreover is associated with disease progression, metastasis, and drug resistance in various cancers (27–31), but the role of Gal-3 in leukemia has remained largely unknown.

Results

Identification of Gal-3 as Candidate Mediator of Leukemia Proliferation and Drug Resistance Caused by BMME. Leukemic cells are supported not only by BMSCs (and their secretion) but also by ECM (13, 32). We first used coculture with HS-5, a BMSC-derived cell line, to examine whether the acquisition of resistance to cell death by TKIs or by genotoxic agents is induced in Ph-positive (Ph^+) CML cell lines (MYL, K562, BV173, and KCL22). HS-5, an immortalized human BMSC-derived cell line, potently secretes various hematopoietic growth factors (33). The coculture rendered both MYL cells and K562 cells partly resistant to TKIs, doxorubicin (DOX), cytarabine (CA), etoposide (i.e., VP16), and vincristine (VCR). BV173 cells, which are primarily resistant to induction of cell death by TKIs, did not become more resistant to IM and Das as a result of coculture with HS-5, but they acquired resistance to cell death induced by DOX, CA, VP16, and VCR. KCL22 also acquired resistance to cell death by DOX (Fig. S1*A*). Ph-negative (Ph^-) cell lines and Jurkat T (i.e., Jurkat) and HL60 cells also acquired resistance to cell death by DOX by the coculture with HS-5 (Fig. S1*B*). We next used microarray-based assays to investigate the changes in gene expression profiles in MYL cells as a result of coculture with HS-5 and adhesion to fibronectin (FN). In MYL with HS-5 or MYL with FN, 902 and 910 genes were up-regulated more than 2.0-fold, respectively, whereas 563 and 550 genes were down-regulated by less than half of their expression levels, respectively, in comparison with levels of control (Fig. S1*C* and Table S1).

Author contributions: J.K. and M.T. designed research; M.Y.-S., J.K., E.A., H.N., T.K., Y.M., N.S., Y.S., M.K., R.N., K.A., T.T., S.H., and T.M. performed research; K.A., N.U., Y.K., and T.M. contributed new reagents/analytic tools; M.Y.-S., J.K., E.A., H.N., T.K., Y.M., N.S., Y.S., M.K., R.N., T.T., N.U., Y.K., S.H., and T.M. analyzed data; and M.Y.-S., J.K., and M.T. wrote the paper.

The authors declare no conflict of interest.

*This Direct Submission article had a prearranged editor.

[1]To whom correspondence should be addressed. E-mail: junkuro@koto.kpu-m.ac.jp.

This article contains supporting information online at www.pnas.org/lookup/suppl/doi:10.1073/pnas.1111138108/-/DCSupplemental.

Among the 284 genes commonly up-regulated in MYL with HS-5 and MYL with FN, we focused on Gal-3 as one of the candidate mediators of BMME-mediated leukemia proliferation/protection because of its pleiotropic cellular function, the interaction with cell signaling molecules downstream of Bcr-Abl TK (Fig. S1*D*), and the association with progression of various cancers (27–31). Because the levels of *galectin-3* mRNA increased 3.84-fold as a result of coculture with HS-5, and 2.83-fold as a result of adhesion to FN in MYL cells, it was likely that Gal-3 was induced by cell adhesion and was further increased by HS-5–derived soluble factors. The induction of Gal-3 by the coculture with HS-5 was also confirmed at the protein level not only in MYL cells, but also in all leukemic cell lines examined regardless of their Ph status, whereas Gal-3 protein expression was absent or extremely low in normal liquid culture (Fig. 1*A*), suggesting that Gal-3 is especially inducible in the presence of BMME components in leukemic cells.

Gal-3 Is Highly Expressed in Primary Treatment-Naive CML Cells in BM. We next investigated the expression of Gal-3 in BM-derived primary leukemic cells from 25 Ph^+ leukemias (20 CMLs and five acute leukemias) and six Ph^- patients with acute leukemia. Of the leukemic cells of 20 patients with CML, those of all but one Ph^+ patient with blast crisis phase leukemia were positive for Gal-3. Ph^+ cells from CML in chronic phase (CP) were especially highly positive for Gal-3 expression. In contrast, the frequency of Gal-3–positive cells from most patients with acute leukemia was as low as that of BM hematopoietic cells from healthy volunteers, regardless of Ph status (Table S2 and Fig. 1*B*). In normal BM, cells of myeloid/monocytic series, but not of lymphoid or erythroid series, were positive for Gal-3. These results suggest that Gal-3 expression in the BM milieu is more predominant in CML, especially in CML-CP.

Gal-3 Overexpression Promotes Cell Proliferation and Chemotactic Cell Migration and Confers Drug Resistance to Leukemic Cells in Vitro. To characterize the role of Gal-3 in CML, we generated Gal-3 stably overexpressing MYL (MYL/G3) and K562 (K562/G3) subcell lines (Fig. S2). Gal-3 overexpression conferred moderately higher in vitro proliferation potency to both cell lines in medium containing 10% FCS as well as in low-nutrient 1% FCS-containing medium (Fig. 2*A*), whereas the growth of cells transfected with the mock plasmid was not significantly different from that of their respective parental cells. Both MYL/G3 and K562/G3 were less sensitive than their respective parental cells to cell death induced by TKIs as well as by conventional anticancer agents (Fig. 2*B* and Fig. S3*A*). Gal-3–overexpressing Ph^- Jurkat/G3 cells were also less sensitive to conventional anticancer agents (Fig. S3*B*). This diminished sensitivity to cell death caused by chemotherapeutic agents was caused by a reduction in apoptosis (Fig. 2*C*). In contrast, the drug sensitivity of cells transfected with the mock plasmid was not significantly impaired. To confirm that MYL/G3 acquired a drug-resistant phenotype as result of Gal-3 overexpression, we examined the effect of an inhibitor for Gal-3, fractionated citrus pectin powder (FPP) (34), on MYL cells and MYL/G3 cells. MYL and MYL/G3 showed similar sensitivity to cell death induced by FPP, whereas the addition of FPP overcame resistance to IM-induced cell death in MYL/G3 cells (Fig. 2*D*). Furthermore, the addition of FPP overcame HS-5–induced resistance against IM in MYL cells (Fig. S3*C*). We also investigated the role of Gal-3 in cell migration of leukemic cells by using conditioned medium (CM) from HS-5 cells (CM/HS-5) as the source of BMSC-derived chemotactic stimuli. CM/HS-5–stimulated cell migration of MYL cells and Gal-3 overexpression further promoted chemotactic and nonchemotactic cell migration in MYL cells (Fig. 2*E*). These findings revealed that Gal-3 overexpression promotes cell proliferation, multidrug resistance, and cell migration in CML cells.

We also examined the involvement of extracellular Gal-3 in the resistance to cell death by chemotherapeutic agents and in the cell migration ability of leukemic cells. Gal-3 concentrations in CM from MYL (CM/MYL), CM from MYL/G3 (CM/MYL/G3), CM from K562 (CM/K562), and CM from K562/G3 (CM/K562/G3) were 0.25 ng/mL, 0.77ng/mL, 0.19 ng/mL, and 9.49 ng/mL, respectively. The addition of recombinant human Gal-3 protein (rhGal-3; ProSci) up to 10.0 ng/mL did not confer CML cell lines more resistance to IM or DOX (Fig. S4*A*), and did not promote cell migration of leukemic cell (Fig. S4*B*), indicating that intracellular Gal-3 expression is essential for the higher resistance to apoptosis and the higher cell migration ability of leukemic cells.

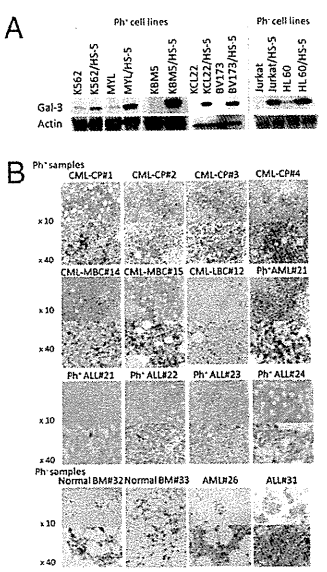

Fig. 1. Gal-3 expression in CML cell lines and primary CML cells. (*A*) Induction by coculture with HS-5 in CML cell lines. (*B*) Immunohistochemical staining of Gal-3 in patient-derived BM samples. Data are representative of the results for all patients examined (Table S2). LBC, lymphoid blast crisis; MBC, myeloid blast crisis.

CM from Gal-3–Overexpressing CML Cells Contains More Proliferative Factors for Leukemic Cells and BMSCs. Leukemic cells excrete growth factors, which stimulate the growth of adjacent leukemic cells as well as BM supporting cells via autocrine and paracrine loops, and thereby create a malignant niche (35). To investigate the involvement of Gal-3 in this scenario, MYL cells or HS-5 cells were cultured with media containing various ratios of CM/MYL and CM/MYL/G3 individually. MYL cells and HS-5 cells proliferated more at higher concentrations of CM/MYL/G3 (Fig. 3), indicating that MYL/G3 cells excrete more growth factors for both MYL cells themselves and BMSCs. These findings were the same for K562 and K562/G3 (Fig. S5). In contrast, the addition of rhGal-3 did not enhance the cell proliferation of MYL or HS-5 cells (Fig. 3 *C* and *D*), suggesting that an undefined soluble factor other than Gal-3 promotes the growth of leukemic cells and HS-5.

Molecular Sequelae Following Gal-3 Overexpression in Leukemic Cells. Coculture with HS-5 and enforced Gal-3 overexpression led to the activation of Akt and Erk in MYL and K562 (Fig. 4*A*). Moreover, coculture with HS-5 and Gal-3 overexpression resulted in the accumulation of Mcl-1, a member of the antiapoptotic Bcl-2 family of proteins, in MYL and K562, as well as a slight increase of Bim_{EL}, a proapoptotic BH3-only protein (Fig. 4*B*). This accumulation of Bim_{EL} may be the result of the accumulation of Mcl-1, which binds to Bim_{EL} in cytoplasm (36, 37). Although recent studies have identified Gal-3 as the substrate of c-Abl in solid cancers (38, 39), Gal-3 expression was not reduced by TKI in MYL and MYL/G3 (Fig. 4*C*), indicating that Gal-3 expression does not depend on Bcr-Abl TK activity in CML cells.

In Vivo Role of Gal-3 in Leukemia. Finally, we examined the in vivo role of Gal-3 in leukemia by studying a mouse CML model transplanted with MYL/mock cells (group A) or MYL/G3 cells